Fall 12-20-2013

Wave transformation at a saltmarsh edge and resulting marsh edge erosion: observations and modeling

Kevin J. Trosclair
University of New Orleans, kjtroscl@uno.edu

Wave transformation at a saltmarsh edge and resulting marsh edge erosion: observations and modeling

A Thesis

Submitted to the Graduate Faculty of the
University of New Orleans
in partial fulfillment of the
requirements for the degree of

Master of Science
in
Earth and Environmental Sciences

by

Kevin Joseph Trosclair

B.S. Louisiana State University, 1995

December, 2013

Acknowledgement

I would like to thank Dr. Ioannis Georgiou, my faculty advisor, for making this thesis possible. First, this work could not be realized had Dr. Georgiou not taken a chance on a very persistent undergraduate student with a nontraditional background. Nor would it be possible had he not taken the effort to secure the funding necessary for this work. I am also grateful for numerous opportunities to engage in many different research activities beyond the focus of my primary work that have expanded my knowledge and allowed me to develop a skill set that will assist me throughout my career. Also for being flexible and allowing me to pursue academic activities outside my area of research, and for occasionally being rigid to help me stay on task when needed. And finally, for giving countless hours of his time to discuss my research as well as many other topics.

My committee members Drs. Denise Reed and Mark Kulp lent their time, patience and understanding while I was preparing this document. Dr. Reed was instrumental in the first steps of this journey, as my decision to leave fulltime employment and pursue a degree in earth science was confirmed after completing an Introduction to Environmental Sciences course she instructed. I should also thank Dr. Kulp for giving me the opportunity to assist with so many Structure field trips and for demonstrating how a field trip should be run. Also, thanks to Dr. Mike Miner for his advice and guidance when I was applying to graduate school. I cannot leave out Linda Miller and Jessica Hebert who were always available to help when needed, and Alexander Falster for being Al. I should also thank Chris Esposito and Scott Wessels, former graduate students who provided some great insight into what I could expect being a graduate student at UNO. And special thanks to Dallon Weathers, for taking the time to answer trivial GIS question and showing me most of what I know about field work. The Coastal Protection and

Restoration Authority (CPRA) for providing financial assistance through the Coastal Science Assistantship Program (CSAP) administered by Louisiana Sea Grant, and finally the United States Geological Survey (USGS) Northern Gulf of Mexico Program (NGOM) and the Pontchartrain Institute for Environmental Sciences (PIES) for sharing financial support to cover all field observations for hydrodynamics, marsh erosion, elevation and bathymetric surveys including analysis.

Table of Contents

List of Figures

List of Tables

Abstract

This study examines wind generated waves during winter storms, their transformation/attenuation near the marsh edge, and the resulting saltmarsh edge erosion. A simple numerical model for wave generation, transmission and marsh edge erosion was developed and validated against observations from Lake Borgne, Louisiana. Results suggest that meteorological conditions modify the local water depth via wind or wave setup and atmospheric pressure, thus exerting a first order control on the location of wave attack, which in turn determines the type of wave forces (shear vs. impact) that dominate the erosion process. Scarp failure follows, at a location determined by water level, creating multiple erosive scarps and terraces. High measured erosion, likely due to marsh edge destabilization followed by subsequent frontal passage forces differential marsh erosion, exposing underlying substrate to further erosion. A conceptual model for marsh edge retreat is developed using these observations and supported further by model predictions.

Marsh Edge Erosion; Wind Wave Attenuation; Winter Storms; Field Observations; Numerical Modeling

Introduction

Coastal wetlands support a variety of natural resource-based industries that are economically important and valued at several billion dollars annually, which includes recreational and commercial fishing, eco-tourism and the petroleum industry (Day et al., 1997; LCWCRTF, 2010). In addition to providing direct economic benefits, coastal wetlands have the capacity to function as a storm buffer to inland communities and infrastructure by absorbing wave energy thus providing protection from wind-generated waves (Leonard and Reed, 2002; Neumeier and Ciavola, 2004; Möller, 2006; Möller et al., 2011). However, protection varies spatially and temporally which demonstrates a non-linear relationship between the characteristics of ecosystems and their protective effects (Koch et al., 2009; Barbier et al., 2008). Barbier et al., (2013) directly linked hydrodynamic conditions such as wave height and storm surge to economic damage analysis to better demonstrate the value of wetlands during storms.

Louisiana contains 40 percent of the intertidal coastal marshes in the contiguous United States (Williams, 1995) , and over the last century has experienced widespread losses (Barras et al., 2003; Barras et al., 2008; Williams, 1995; Dahl, 2000). Since the 1930s, an area of nearly 4900 km^2 of wetlands was converted to open water, with the average annual loss rate (from 1956 to 2006) ranging from 90 km^2/y to 115 $km^{2/}y$ (Barras et al., 2003; Barras et al. 2008; Couvillion et al., 2011). Multiple factors contribute to wetland loss including a lack of mineral sediment via riverine input, hydrologic disruption, saltwater intrusion and physical erosion, which are a result of both anthropogenic and natural forces and ultimately lead to the conversion of wetlands to open water (Boesch et al., 1994; DeLaune et al., 1994; Day et al. 2007; LCWCDTF, 2010; Day et al., 2011). The coalescing of interior ponds create larger open bays (Day et al., 1994; Ashton

et al., 2009) that are exposed to more energetic events including both hurricanes and cold fronts (Fagherazzi et al., 2007; Fagherazzi and Wiberg, 2009).

The wave climate along the Louisiana coast is a product of seasonal wind patterns and the passage of tropical and extratropical storms (Georgiou et al., 2005). The Northern Gulf Coast region is affected by a high incidence of tropical cyclones (Muller and Stone, 2001), however, cold fronts are often more damaging in terms of their erosive ability, compared to hurricanes, primarily because of their high frequency of occurrence (Mossa and Roberts, 1990). In an average year, 20 to 40 cold fronts pass through coastal Louisiana (Roberts et al., 1987; Chaney, 1998). These systems can be defined as narrow transition zones between two air masses of different densities, characterized by changes in wind speed, direction, barometric pressure, temperature, and humidity (Mossa and Roberts, 1990). The pressure gradient at the leading edge of these frontal systems controls the intensity and transfer of momentum/energy to the coast, which is manifested in the form of strong winds, large waves, and rapid changes in water levels (Pepper and Stone, 2004; Li et al., 2010). Keen (2002) identified cold fronts as major factors in the short-term evolution of estuaries along the northern Gulf of Mexico in terms of (1) waves and their continuous interaction with the bed, and (2) estuarine circulation due to shifting winds. During frontal passage, estuaries and bays that are connected to the ocean by well-defined inlets exchange as much as 40% of their volume which significantly affects their water level (Feng and Li, 2010). Onshore winds during pre-frontal conditions promote this exchange and increase the volume of water flowing through tidal inlets into the bays, as well as increasing salinity (Li et al., 2010; Schindler, 2010).

Wind waves in shallow coastal bays during cold fronts are typically depth-limited (i.e. wave height is controlled by interaction with the sea-bed), are steep, and often exhibit high

frequencies and nonlinear shapeform (i.e. their shape cannot be described by linear wave theory) (Keen, 2002; Stone et al., 2004). In shallow water, wave speed is governed by water depth rather than wavelength, $c = (gd)^{0.5}$, and, therefore wave speed decreases near the shoreline (Holthuijsen, 2007). This decrease in speed shortens wavelength and increases wave height, resulting in larger and steeper waves, which in turn increases the number of wave crests with in a given distance. Since wave energy (per unit area over one wavelength) is proportional to the square of the wave height, $E = \frac{1}{8}\rho g H^2$, increasing the amplitude of a wave increases the energy transported by the wave (Knauss, 1996). Since steep waves can deliver more wave energy to the shoreline they are believed to be responsible for the chronic shoreline erosion along coastal bays (Keen, 2002; Stone et al., 2004; Schwinner and Pizzuto, 2000; Fagherazzi et al., 2007).

Scientific Research Questions

The specific questions to be answered by this study are

1. Do the short period, high amplitude waves generated during cold fronts account for more erosion to the marsh edge than waves generated during the remainder of the year?
2. What is the impact of water/tidal level fluctuations on the wave transformation processes, and what are the feedback mechanisms with the marsh edge/scarp?
3. How does the marsh edge respond to the erosive forces that result from wave energy dissipation in terms of short term erosion rates?

Scientific Hypothesis

H1 Short period, high amplitude wind waves generated during cold fronts transfer a greater amount of energy to the marsh edge than waves generated during fair weather conditions.

H2 The energy transferred to the marsh edge during winter storms accounts for a greater proportion of the observed shoreline erosion compared to energy transferred during fair weather condition.

Background

Previous Work

Marsh Edge Erosion

Wave attenuation by coastal vegetation has been the focus of much research in recent years (Wayne, 1976; Knutson et al., 1982; Fonseca and Cahalan, 1992; Moeller et al., 1996; Massel et al., 1999; Möller et al., 1999; Möller and Spencer, 2002; Cooper, 2005; Mazda et al., 2006; Möller, 2006; Quartel et al., 2007; Möller et al., 2011; Yang et al., 2012; Wu, 2011; Wu, 2012). Studies of wave attenuation in saltmarshes have shown that vegetated wetlands can attenuate wave energy more effectively than un-vegetated sand or mudflats, and most wave energy dissipation occurs in the first few meters of the permanently vegetated saltmarsh (Möller and Spencer, 2002). Wave energy dissipation was shown to be two times higher at scarped marsh edges than sites without the abrupt transition between the mudflat and saltmarsh (Möller and Spencer, 2002).

Saltmarshes evolve vertically, through the processes of deposition (organic and inorganic), surface erosion and relative sea level rise while horizontal evolution is a result of vegetation colonization and lateral erosional processes. Considerable attention has been focused on understanding the controlling processes responsible for the accretion or erosion of saltmarsh surfaces with field observations and numerical models (Delaune et al., 1983; Boumann et al., 1984; Reed, 1989; Nyman et al., 1990; Cahoon and Reed, 1995; Day et al., 1994; Morris et al., 2002; D'Alpaos et al., 2007; Kirwan and Murray, 2007; Mudd, 2011). However, lateral erosional mechanisms have not been as well studied; even though marsh edge erosion is one of the primary mechanism by which coastal marshes are being lost (van Eerdt, 1985; Penland et al., 2000;

Schwimmer and Pizzuto, 2000; Schwimmer, 2001; van de Koppel et al., 2005; Wilson and Allison, 2008; Feagin et al. 2009; Mariotti and Fagherazzi, 2010; Marani et al., 2011). Marsh edge erosion is a complex process and is dependent on a variety of factors (soil characteristics, root effects, and bioturbation, etc.); however studies suggest that waves are the chief driver of saltmarsh edge erosion (Moeller et al., 1996; Möller et al., 1999; Schwimmer and Pizzuto, 2000; Watzke, 2004; Wilson and Allison, 2008; Feagin et al. 2009; Mariotti and Fagherazzi, 2010; Mariotti et al., 2010). Studying the relative importance of these factors, Feagin et al. (2009), suggested that it is the soil type rather than the vegetation that controls marsh edge erosion, whereas Fagherazzi et al. (2012), argue that vegetation does play a role in the resulting morphology of the marsh profile. Francalanci et al. (2013) has recently shown in wave flume experiments that vegetation roots prolonged the time needed to erode equal amounts of sampled marsh material. Few field studies directly address marsh edge erosion in southeast Louisiana. Watzke (2004) examined low-energy fringing marshes in Louisiana and concluded that these marshes undergo substantial geomorphological change due to erosion from locally generated high-frequency waves produced during cold fronts. Wilson and Allison (2008) studied shoreline retreat in southeast Louisiana and found marsh edges adjacent to open (shallow) bays are vulnerable to wave attack and proposed an equilibrium profile model for retreating marsh shorelines that is driven by marsh edge erosion and local subsidence. Ellison (2011) modified the model suggested by Wilson and Allison (2008) to account for the presence of shell fragments within the substrate and on the marsh platform and explains marsh edge morphology found in the eastern Biloxi Marsh in Louisiana. Several studies used numerical modeling to describe marsh edge erosive processes. Fagherazzi et al. (2012) used a numerical model to simulate shoreline erosion rates and showed that a scarped marsh exhibited a higher erosion rate per unit energy,

compared to a non-scarped edge. Furthermore, Tonelli et al. (2010) used a numerical model to evaluate the effects of nonlinear shallow water waves on marsh boundaries as a function of tidal elevation and wave height, showing that wave thrust/energy increases with tidal elevation until the marsh is submerged, then rapidly decreases once inundated.

It is well documented that wetlands have a greater capacity to attenuate waves than do non-vegetated shorelines and that most attenuation occurs in the first few meters of the marsh or more specifically along the marsh edge. However, most prior studies measure attenuation rates as the average dissipation over tens of meters along transects that include the marsh edge. This study will: 1) examine wave transformation/attenuation and resulting erosion at the marsh edge with observations of wind generated waves during winter storms in the Biloxi Marsh, adjacent to Lake Borgne; 2) develop a simple numerical model for wave generation, transmission and marsh edge erosion; 3) validate against our field observations, (4) use the model to gain insight into marsh edge erosion processes in coastal Louisiana, and (5) develop a conceptual model describing marsh edge retreat based on observations and predictions from this study, supplemented further by long-term records of retreat (Martinez et al., 2009) in the Biloxi Marsh.

Regional Setting

The Mississippi River delta plain (MRDP) developed during the Holocene and covers an area of 30,000 km^2 (Coleman et al., 1998), is comprised of several delta complexes which in turn are composed of multiple delta lobes that are fed by many distributary channel networks of the Mississippi River (Roberts, 1997). The St. Bernard delta complex was active until approximately 1,500 years BP (Tornqvist et al., 1996) and extends east from Lake Pontchartrain to the Chandeleur Islands (Frazier, 1967). After abandonment, fluvial dominance gave way to

marine processes resulting in the reworking of the deltaic sediment leading to the formation of the Chandeleur Islands and the St Bernard Wetlands. The St. Bernard Wetland Area (SBWA) encompasses 146,450 acres of marshes, bayous, shallow bays and ponds that extends from the Mississippi River Gulf Outlet (MRGO) channel north to Mississippi Sound (Penland et al., 2002). These marshes maintain elevation within the tidal range through a balance between mineral sediment accumulation and peat formation versus submergence and erosive forces (Nyman et al., 1990; Day et al., 1994). When this balance is interrupted wetlands are lost. Penland et al. (2000) classified wetland loss in Louisiana as either inland or shoreline losses. Although nearly 70% of total wetland loss was attributed to interior processes, wetland losses around Lake Borgne is the result of shoreline losses with marsh edge erosion by wave processes the primary mechanism of shoreline retreat (Penland et al., 2000; Penland et al., 2002; Couvillion et al., 2011; Wilson and Allison, 2008).

Study Site

The study site is located on the eastern shore of Lake Borgne in the Biloxi Wildlife Management Area, Louisiana (Figure 1). Lake Borgne has a surface area of 730 km² and an average depth of 3 m (USEPA, 1999). Lake Borgne has an oblong shape which trends from southwest to northeast and opens into Mississippi Sound. The shoreline at the site is oriented facing the northwest along the lake's minor axis. The fetch across the lake ranges from 16 to 22 km with the longer fetches facing the west-northwest. The wetlands surrounding the site were classified by the Coastwide Reference Monitoring System (CRMS) in 2012 as a saline marsh dominated by *Spartina alterniflora* (68%) and *Juncus romerianus* (http://www.lacoast.gov/crms2/Home.aspx). The mean tidal range is approximately 0.39 m while the mean diurnal range is 0.45 m (USEPA, 1999). The site was chosen because of the

shoreline orientation and the significant fetch across Lake Borgne which would increase the probability that wind-induced water setup and large wind waves will inundate the marsh. The nearest CRMS station (CRMS4572) to the study site reports an elevation change 0.11 cm/y greater than RSLR.

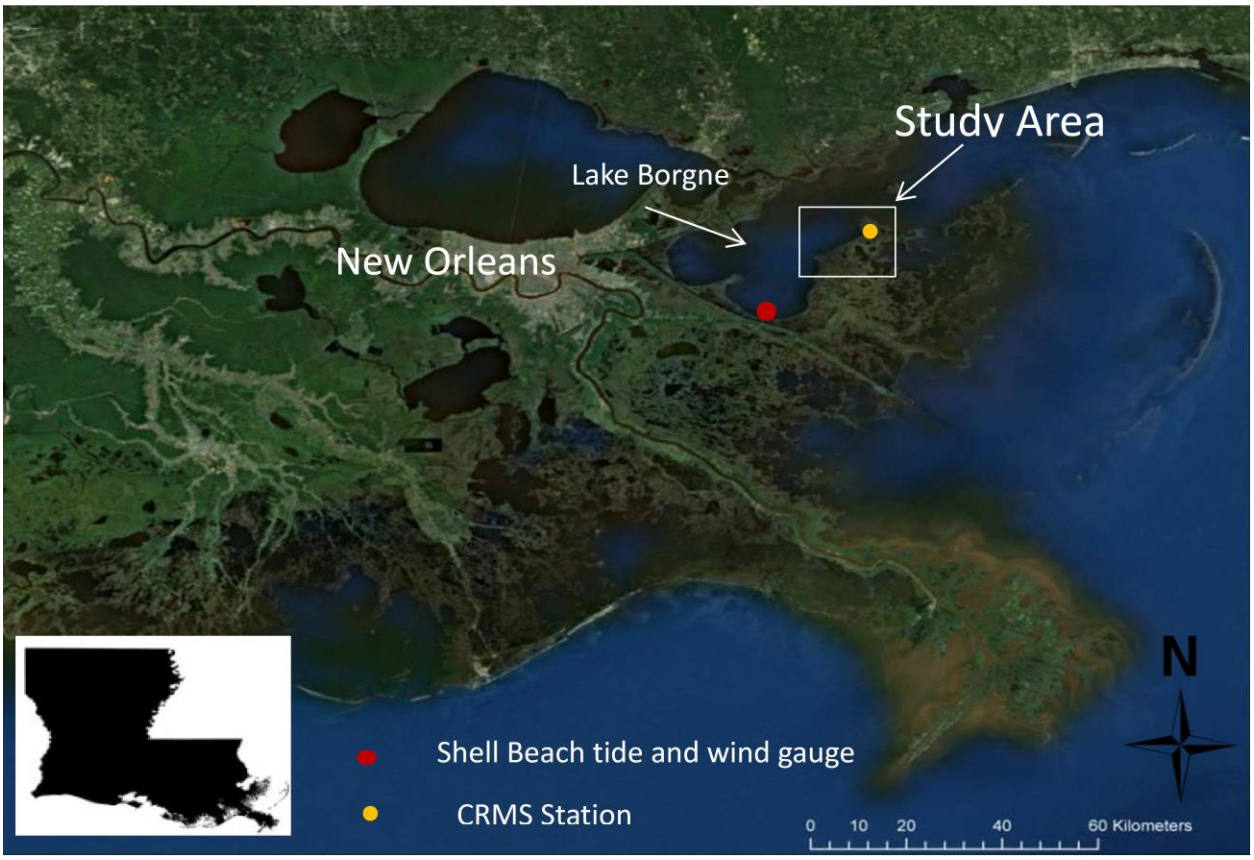

Figure 1 Mississippi River delta plain highlighting the study site for this research (white box) on the eastern shore of Lake Borgne in the Biloxi Wildlife Management Area, Louisiana; The location of the nearest CRMS station is shown (yellow circle), as well as the Shell beach tide gauge (red circle).

Methods

A preliminary survey was used to evaluate selected sites to determine the likelihood of inundation during a winter storm event. Marsh and water level elevations were taken at selected sites via Differential Global Positioning System (DGPS) and were correlated to water levels recorded by a NOAA tide gauge located 17 kilometers away at Shell Beach, LA. (Figure 1), and then used to hindcast conditions at the site to predict the likelihood of inundation. This was accomplished by correlating water levels measured at the study site with water levels obtained from the Shell Beach gauge to determine the offset between water surface elevations. The marsh elevations at the site were performed during calm conditions, and as such the effects of setup were most likely not present at either site. This allows for a more accurate calculation of the potential setup at each site resulting from a storm, thus providing a better estimate of the inundation depth. Measurements from three different surveys were used to calculate an average offset of 0.046 (+/- 0.014) meters NAVD88. This offset was applied to the long-term water level records obtained from Shell Beach to estimate the water level and inundation at the study site in meters NAVD88. The study site was chosen after the preliminary survey, and then three field campaigns followed (Table 1).

Table 1 Field visit dates and activities

Survey Date	Activities
04/11/2012	Preliminary survey
12/14/2012	Topographic survey ADV deployment Erosion pin deployment
12/22/2013	ADV recovery Erosion measurements
04/30/2013	Topographic survey Bathymetric survey Erosion measurements

Topographic Survey

To define the marsh edge morphology, elevation measurements were conducted along a shore normal transect in the NNW direction (Figure 2). Measurements were taken on the first site visit (12/14/2012), and during the last visit to the site (4/30/2013) (Table 1). Elevations were at 2 meter intervals with additional points as needed to better define the marsh scarps and/or platforms. Data from the topographic and bathymetric survey was used to determine the elevations of marsh features as well as the elevations where the instruments were deployed, and to create a continuous cross-shore profile of the study area from the marsh platform to the Lake Borgne seabed. The surveys also served as an additional dataset documenting horizontal marsh retreat and overall profile evolution. The exact (cm scale resolution) location of the shoreline was determined during the final survey by walking along the marsh/water interface with the DGPS receiver. This GPS trace provides the most up to date position of the shoreline at the study site.

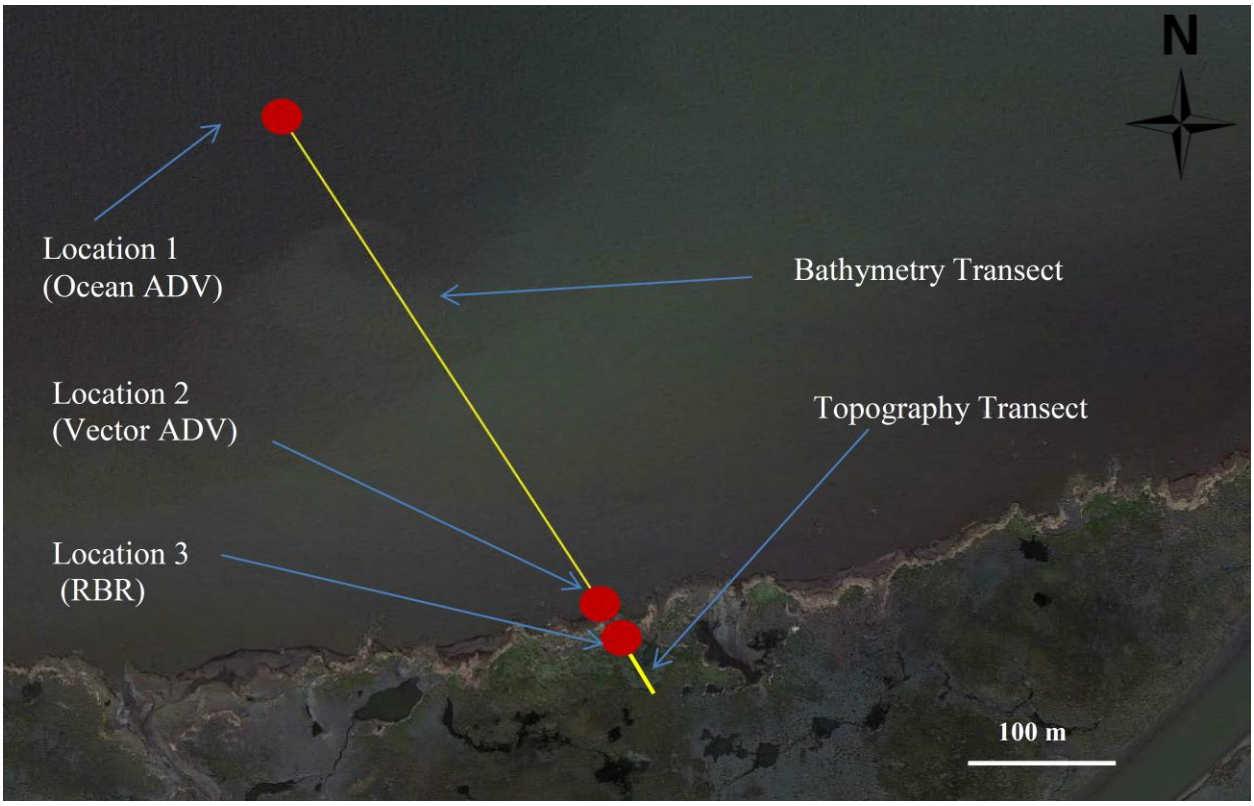

Figure 2 Aerial photograph of the study site showing the northwest facing shoreline on the eastern shore of Lake Borgne. The locations of deployed wave instruments are marked by the red dots and the location and direction of the bathymetric and topographic survey lines are shown in yellow solid line.

The site elevations were obtained with two Thales Navigation Z-MAX dual frequency Differential Global Positioning System (DGPS) operating as base and rover units. This method enables sub-centimeter accuracy horizontally and ~1 cm accuracy vertically through post processing. The base station data were processed using the Continuously Operating Reference Stations (CORS) system managed by the National Geodetic Survey (NGS). GNSS data post-processed using CORS data improves the precision of coordinate measurements, both horizontally and vertically relative to the National Spatial Reference System (NSRS) (NGS, 2006). The rover data was post processed using NovAtel-Waypoint's GNSS Post-Processing Software GrafNav, which performs differential processing using the base station data, the post-

processed coordinates obtained from the NSRS and satellite clock and orbit information to calculate a solution for the rover data to facilitate better accuracy. The base station consists of a GPS unit with and external choke ring antenna placed 2 m above a temporary benchmark installed by inserting an aluminum rod approximately two meters into the marsh to provide a stable point for the base station and antenna to rest. The second GPS was used as a rover unit and was configured with a portable antenna module and mounted on a portable monopod, 1.431 m above the monopod's measuring surface.

Water surface elevations at the site were measured in meters NAVD88 during calm meteorological conditions (when the effects of wind/wave setup, atmospheric pressure etc. are minimal) and correlated with water level elevations obtained from the NOAA station at Shell Beach in order to tie the data to a common datum. This method permitted the use of the Shell Beach station as a proxy for conditions experienced at the study site, and for further use in wave hindcast and forecast analysis. This provides a local inundation depth for more accurate predictions of wave transformation and subsequent edge erosion.

Bathymetric Survey

The surveys were conducted with RV Mudlump, equipped with an Odom Hydrographics Hydrotrac Single Frequency Portable Hydrographic Echo Sounder, an Odom Hydrographics TSS DMS-05 Motion Sensing Unit (MSU), a Thales Navigation Z-MAX dual frequency DGPS, and an onboard computer running HYPACK® Hydrographic Survey and Processing Software. Three cross-shore profiles were surveyed spaced 50 m apart and were connected by two along-shore lines, at 100 m intervals. The along-shore lines are referenced with the cross-shore lines and provide a quality check for consistency in sounding values. The fathometer operates at a

frequency of 200 kHz and has a vertical resolution of 0.01 meters. High frequency transducers have a better resolution than lower frequency transducers and are typically used for shallow water. The MSU corrects the stream of sounding data in real time for heave, pitch, and roll created by waves acting on the vessel while under way. The vessel based GPS functions as a rover unit and collects GNSS information simultaneously with the GPS receiver at the nearby base station. HYPACK® Hydrographic Survey and Processing Software was used to collect the data steam and to combine the real time and post processed corrections into a high resolution mapping of the nearshore area. To extend the elevation measurements at the site from the marsh platform to Lake Borgne, depth soundings were collected along the cross-shore profile extending from the topographic transect toward the bathymetric profile (Figure 2).

Short-term erosion measurements

Marsh edge erosion was measured using erosion pins (Haigh, 1977; Priestas and Fagherazzi, 2011), inserted horizontally into the marsh scarp. Pins were placed at four locations at the site, two along the transect line as well as two other location to serve as a backup and to provide duplicate measurements for statistical inferences (Figure 3). The pins were constructed of metal bars, 1.5 cm wide and 45 cm long. Two pins were placed at each location and inserted approximately 35 cm into the marsh edge on 12/14/2012, and recorded erosion measurements on 12/22/2012 (8 days), and on 4/30/2013 (4 months).

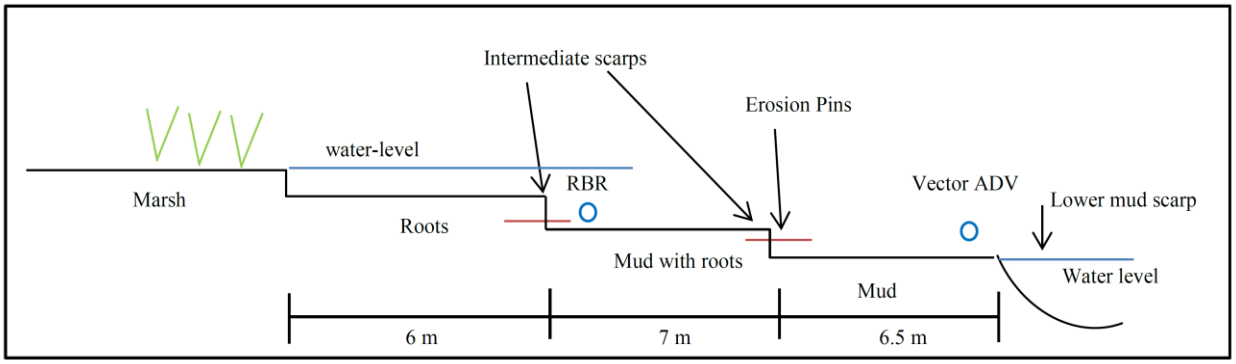

Figure 3 Cartoon of a cross-shore section of the study site showing multiple erosional scarps and terraces. The location of the deployed instruments is marked by the blue circles and the red lines mark the location where the erosion pins were inserted. The blue lines represent the water level during high and low water events.

Wave data collection and analysis

Wave and current meter deployments

An array of bottom-mounted Acoustic Doppler Velocimeters (ADVs) were deployed on December 14, 2012 at three locations along the planned transect. A SonTek Acoustic Doppler Velocimeter (Ocean ADV) was deployed 400 m offshore in approximately 2.6 m of water mounted on an Ocean Science Barnacle deployment platform 0.22 m above the bed (Location 1; Figure 2 & Figure 3). The Ocean ADV recorded wave climate and currents every 30 minutes from 12/16/2012 through 12/22/2012. Each wave burst measured 4096 water elevations at 4 Hz, which results in a burst length of 1024 s (17 min). The Ocean ADV was used to resolve the incoming storm and wave energy from the receiving basin during the deployment period. In addition, a Nortek Vector Field Acoustic Doppler Velocimeter (Vector ADV) was placed on the lower mud flat at the edge of the lower mud scarp (Figure 3). The Vector ADV recorded waves and currents every 30 min, sampling at a frequency of 16Hz. Each wave burst collected 12,288

water elevations which results in a burst length of 768 s (12.8 min) consistent with observations at other deployment sites. The Vector ADV has two components, a canister that contains the instrument's electronics and pressure sensor and a transducer probe that sends and receives ultrasound pulses. The canister was mounted securely flush to the mud flat using two 120 cm metal rods (Figure 3). The velocity probe is connected to the housing with a flexible cable, and it was mounted to a different metal rod 1 meter from the seaward edge of the mud flat and 10 cm above the bed. The velocity probe was oriented such that the cross-shore velocity was aligned with the heading of the topographic transect. Finally, a RBR-Global TWR-2050 pressure sensor was placed at the edge of the vegetated marsh (Figure 3), and measured waves and tides every 60 minutes by collecting a series of 4096 water elevations measurements at a sampling frequency of 4Hz, which results in a burst length 768 sec (12.8 min). The instrument was deployed 12.5 m. landward of the Vector ADV near the edge of the vegetated marsh platform, and was used to confirm inundation of the marsh and possibly resolve wave dissipation across the transect during storm conditions with sufficient inundation.

Data Analysis

The data was recovered from the instruments and post processed to determine the wave and currents experienced at the site during the deployment period. The data were correlated to meteorological and astronomical data (tides and atmospheric pressure) obtained from NOAA tide gage station 8761305, Shell Beach, Louisiana. Standard wave statistics, (wave height and period) were computed with methods described by Tucker and Pitt (2001). Pressure data (frequency range 0.25-2 Hz) was processed to correct for the attenuation of pressure with depth, then standard spectral and zero-crossing non-directional wave parameters were computed. Velocity data from busts were used to calculate the mean velocity magnitude and the 95^{th}

percentile velocities associated with the incoming waves with positive velocities denoting movement in a shoreward direction.

The wave statistics generated by spectral methods were used to define other characteristics of the wave field such as wave steepness, the degree of nonlinearity, breaking criteria, the type of breaker and were used to validate predicted waves produced by the model. In order to determine these parameters, waves must be classified as shallow, intermediate or deep water wave using the ratio *d/L*, where *d* is the water depth and *L* is the wave length (Table 2). The method used to calculate wave length was developed by Hunt (1979), is given by

$$k = \frac{\left(y^2 + \frac{y}{1+0.666y+0.355y^2+0.161y^3+0.0632y^4+0.0218y^5+0.00654y^6}\right)^{-1/2}}{h}, \quad (1)$$

where,

$$y = 4.03\frac{h}{T^2}. \quad (2)$$

With the wave number *k*, the water depth *h* and wave period *T*, the wavelength can be derived using,

$$L = {}^{2\pi}/_{k}. \quad (3)$$

Table 2 Range of values for the ratio of water depth and wavelength used to classify waves as deep, intermediate or shallow water waves.

d/L > 0.050	Deep Water Wave
0.04 > d/L > 0.50	Transitional Wave
0.04> d/L	Shallow Water Wave

Most waves in the coastal zone are transitional or shallow water waves. In shallow water, wave speed is governed by water depth rather than wavelength therefore wave speed decreases near the shoreline. This decrease in speed shortens wavelength and increases wave height, resulting in larger and steeper waves (Holthuijsen, 2007). Wave steepness increases as waves become nonlinear and is determined by the ratio

$$H/L \quad , \tag{4}$$

where H is the wave height. The degree of nonlinearity can be quantified with the Ursell Number, N_{Ursell}, which combines wave steepness and relative water depth (USACE, 1984; Holthuijsen, 2007). Large N_{Ursell} indicate increased nonlinearity and is given by:

$$N_{Ursell} = gHT^2/h^2 \quad . \tag{5}$$

The Ursell number is also used to determine which wave theory is valid for a given wave (Table 3).

Table 3 Range of values for the Ursell Number which can be used to indicate the degree of nonlinearity of a given wave. The Ursell Number is also use to identify the most appropriate wave theory to describe a given wave.

$N_{Ursell} > 26$	Cnoidal Theory
N_{Ursell} 10-26	Stokes and Cnoidal Theory
$N_{Ursell} < 10$	Stokes Theory
$N_{Ursell} << 10$	Linear Theory

The maximum height a wave can attain before it breaks is related to the water depth. This wave height/water depth relationship is often known as the breaker index, γ and is given by

$$\gamma = 0.78h \, . \tag{6}$$

This is a first order estimate and can be as low as 0.5 or as high as 1.5 based on local bed slope, wave steepness or wind (Holthuijsen, 2007). The depth of water in which waves break is related to the wave height and for shallow water is given by

$$H_b = \gamma\, d \ . \tag{7}$$

The type of breaker can be predicted with the surf similarity parameter or Iribarren number (Battjes, 1974; Holthuijsen, 2007), ξ_b, and for shallow water is given by

$$\xi_b = \tan\alpha / \sqrt{H_{br}/L_o} \quad . \tag{8}$$

where, *tan* α is the local bed slope, and H_{br} is the wave height at breaking. Values for different breaker types are given in Table 4.

Table 4 Iribarren number (ξ_b) or surf similarity parameter can be used to predict or describe breaking waves. The table shows the range of values of ξ_b used to classify breaking wave as spilling, plunging or surging breakers.

Breaker type	ξ_b
spilling	< 0.4
plunging	0.4 - 2.0
surging or collapsing	> 2.0

Model Development

To forecast conditions at the site, the wave environment was modeled using empirical relationships developed by Young and Verhagen (1996) from field observations in shallow environments. This relationship shows the dependence of significant wave height H_w and wave period T_w on the available fetch X_f. Given depth, d and wind speed, U_w, the relationship is given by:

$$\frac{H_w}{U_w^2/g} = 0.17\left[tanh\, A_1\ tanh\left(\frac{B_1}{tanh\, A_1}\right)\right]^{0.87}, \tag{9}$$

$$\frac{T_w}{U_w^2/g} = 7.518\left[tanh\, A_2\ tanh\left(\frac{B_2}{tanh\, A_2}\right)\right]^{0.37}, \tag{10}$$

where,

$$A_1 = 0.493\left(\frac{d}{U_w^2/g}\right)^{0.75},\ B_1 = 3.13\times10^{-3}\left(\frac{x_f}{U_w^2/g}\right)^{0.57}, \tag{11}$$

$$A_2 = 0.331\left(\frac{d}{U_w^2/g}\right)^{1.01},\ B_2 = 5.21\times10^{-4}\left(\frac{x_f}{U_w^2/g}\right)^{0.73}. \tag{12}$$

The effects of wind setup, Z_{sup} on local water levels was included in the wave analysis and is given by the relationship,

$$Z_{sup} = \frac{F'\left(\rho_a C_f U_{OW}^2\right)}{2g\rho_w d} \tag{13}$$

were F' is the effective fetch, C_f is the wind friction coefficient, $\rho a/\rho w$ is the ratio of the density of air to the density of water, and U_{ow} is over water wind velocity at 10 m above the surface (USACE, 1984).

To determine U_w and to characterize the wind distribution at the study site, an hourly time series of wind speed and direction was collected from the NOAA station 8761305, Shell Beach. A wind rose analysis was performed to obtain wind direction, frequency and magnitude for long term analysis. The records were split into two seasons to investigate seasonal trends. Period 1 corresponds to the cold front season (1 November through 30 March), and period 2 corresponds to the remaining part of the year (1 April through 30 October).

After obtaining wave heights with the above relationship a regression analysis was conducted using a 3rd degree regression function to simulate the transformation/transmission of offshore waves moving from the open water to the nearshore environment. The function was fitted to observations recorded at the study site, and was adjusted based on knowledge of inundation and local depth. The resulting wave heights were used to calculate the total and mean wave energy and wave power arriving at the study site (discussed later).

Velocity data was used to calculate local shear stresses to assist in the erosion analysis. The maximum shear stress generated by a wave, τ_w, can be estimated from the relationship,

$$\tau_w = \frac{1}{2}\,\rho f_w U_b^2\,, \tag{14}$$

where ρ is the water density, f_w is a wave friction coefficient and U_b is the maximum wave induced bottom velocity evaluated using linear wave theory and is given by:

$$U_b = \frac{\pi H_w}{T_w\,sinh(kD)}\,, \tag{15}$$

where $k=2\pi/L$ is the wave number. The wave friction coefficient f_w, calculated after methods by Kamphuis (1975) and Fredsoe and Deigaard (1992) is given by:

$$f_{w1} = 0.4(a_w/k_N)^{-0.75}(rough\ bed\ \ a_w/k_N < 50), \quad (16)$$

$$f_{w2} = 0.04(a_w/k_N)^{-0.25}(rough\ bed\ \ a_w/k_N\ > 50), \quad (17)$$

$$f_{w3} = 0.035R_E^{-0.16}(smooth\ bed). \quad (18)$$

with a_w/k_N the relative roughness. We assumed a a_w/k_N of 6.3 as used by Tambroni and Seminara (2012) in a similar environment thus used f_{w1} from above.

To describe the erosion at the marsh scarp we used a formulation proposed by Mariotti and Fagherazzi (2010) that incorporates wave power, *P* into the erosion component in the relationship:

$$\rho_b(D - R)\ , \quad (19)$$

where ρ_b is the sediment density, *D* is the sedimentation rate and *R* is the erosion rate. The erosion rate, *R* is composed of two terms that express erosion due to bottom shear stress from waves and currents and from turbulence generated from wave breaking and is given by,

$$R = R_{shear} + R_{break}\ . \quad (20)$$

The shear component is used to describe erosion from bottom shear stresses that occur below the waves such as the water bottom or marsh surface when inundated and is given by,

$$R_{shear} = \begin{cases} 0 & \tau < \tau_{cr} \\ A(\tau - \tau_{cr})^{\alpha} & \tau > \tau_{cr} \end{cases} \quad (21)$$

where A is the erosion rate, α ranges from 1 for cohesive sediments to 1.5 for loose sediments and τ_{cr} is the critical shear stress needed for erosion to occur. Mariotti and Fagherazzi

(2010) used a formulation of R_{break} which incorporates wave power P, as the energy term to describe the forces acting on vertical surface of a scarped marsh edge and is given by,

$$R_{break} = \begin{cases} 0 & P < P_{cr} \\ \beta(P - P_{cr})^{\alpha} & P > P_{cr} \end{cases}, \quad (22)$$

where P is wave power per unit area, P_{cr} is the critical power necessary for erosion, and β is a calibrating constant. Wave power is the product of wave energy and wave group velocity and is given by linear theory as

$$P = Ec_g \quad (23)$$

with,

$$E = \frac{1}{8}\rho g H^2 \quad (24)$$

and

$$cg = (gd)^{0.5}(1 + 0.75\frac{H}{d})^{0.5}, \quad (25)$$

Although these equations relate to bottom sediment erosion, Mariotti and Fagherazzi (2010) used the wave breaking term, R_{break}, to model marsh edge erosion by setting P equal to the rate of power dissipation of the wave impact force to the marsh scarp. Similar approaches have been used to correlate long term marsh edge erosion to wave power (Schwimmer, 2001; Marani et al., 2011). Values of 3, 5 and 15 watts were used for P_{cr}, with the lower values representing more erodible material in the mudflat and higher values for the more resistant marsh scarp (Mariotti and Fagherazzi, 2010). A value of 1 was used for the exponent α since the site consists of primarily cohesive sediments. Vegetation and sediment characteristics are not

accounted for directly in this approach but are included in β. The β parameter was calibrated with the erosion measurements obtained on the marsh terrace to specify an erosion rate in m/y.

Measured and predicted wave heights collected during the deployment period were used to calculate total wave energy and wave power arriving at the study site (Eq. 23 & 24). Wave power was used with an estimate of β to obtain a preliminary value for R, and then calibrated to correspond to the erosion measured at the site in meters per year (Eq. 22). The calibrated value for β was then used to validate R with predicted wave heights over the second deployment period. A correlation was identified between P and R for both deployment periods then β was adjusted to correspond to the measured erosion over the second (longer) deployment. Once the β parameter was set, it remained unchanged for all future long-term simulations.

Quantitative comparisons of model results were performed based on regression analyses and the index of agreement method. The index of agreement is a method that compares time-dependent predicted and observed variables developed by Willmott (1981). The index of agreement is a statistical approach to measure a model's performance by comparing model estimates or predictions with reliable pair-wise matched observations (Willmott, 1981). A score of 1 indicates perfect agreement whereas a score of 0 suggests no agreement.

Results

Analysis of regional meteorology

Wind climate analysis at Shell Beach, LA was conducted by generating a wind rose which shows the wind frequency for selected magnitudes (magnitude bins) and directions (directional bins) affecting the study site. The results for the most recent 5 year period show dominant wind directions from the north and southeast (Figure 4). While winds have a higher frequency from the southeast, winds from the north contribute a greater percentage of high magnitude winds. The directional distribution and dominance varied from summer to winter seasons. The typical response during the winter season was dominance from the north and northwest and from the southeast (Figure 5), while the remainder of the year produced dominance from the southeast, southwest, and northeast (Figure 5). The shoreline orientation at the study site typically receives incoming winds from the west to the northeast (270°- 45°) influencing the site 43 % (38 %-59 %) of the time for the examined records (2008-2012).

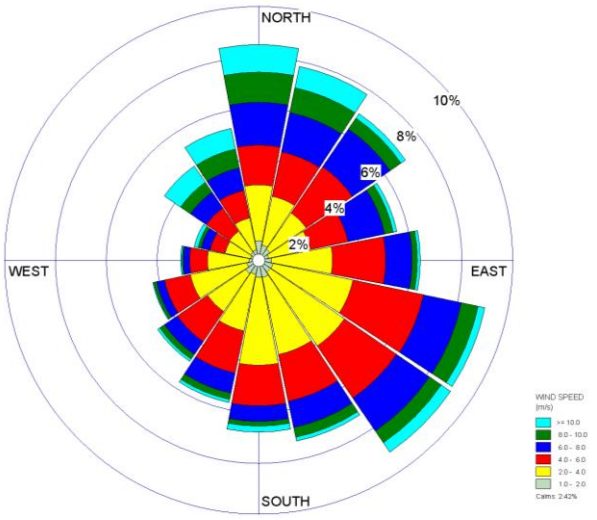

Figure 4 Wind rose showing the wind direction, frequency and magnitude at NOAA station 8761305 in Shell Beach, Louisiana from 2008-2012. Winds are grouped by direction into 22.5 degree bins. The number of wind records in each bin is represented by the distance the bin extends from the center of the wind rose and the magnitude of the winds in each bin is indicated by the range of wind speeds shown in the legend.

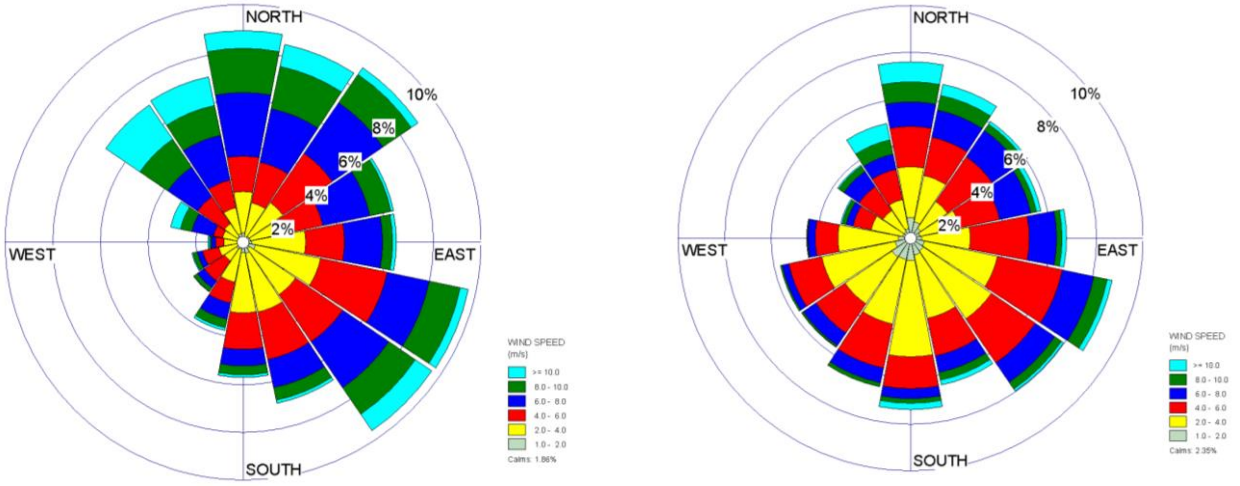

Figure 5 Wind rose showing the seasonal wind distribution at NOAA station 8761305, Shell Beach, Louisiana; a) left - Wind distribution from November 2012 to March 2013 showing dominance form the northwest, northeast and southeast; b) right - Wind distribution from April to October 2012 shows dominance from the southwest to southeast.

Tidal record analysis from the NOAA Shell Beach gauge (n=5yrs) were utilized to obtain the frequency of inundation of the study site by generating a stage duration curve (Figure 6). The cumulative frequency of each water-level measurement was calculated then plotted against water elevation to estimate the frequency of inundation After correlating the tidal data to a common datum (see methods), the elevations of the lower mud scarp, the intermediate scarps and the marsh platform were utilized to derive this frequency. Based on this analysis the lower mud scarp (Vector ADV pressure sensor), the second intermediate scarp (RBR) and the marsh surface would be inundated 88%, 64% and 51% respectively. This is in agreement with an average hydroperiod of 52% (n=4yrs) reported by the CRMS4572 site. This suggests that the site is inundated frequently, allowing wave transformation and transmission onto the marsh environments, thus provides a framework to understand non-linear breaking waves and resulting erosion.

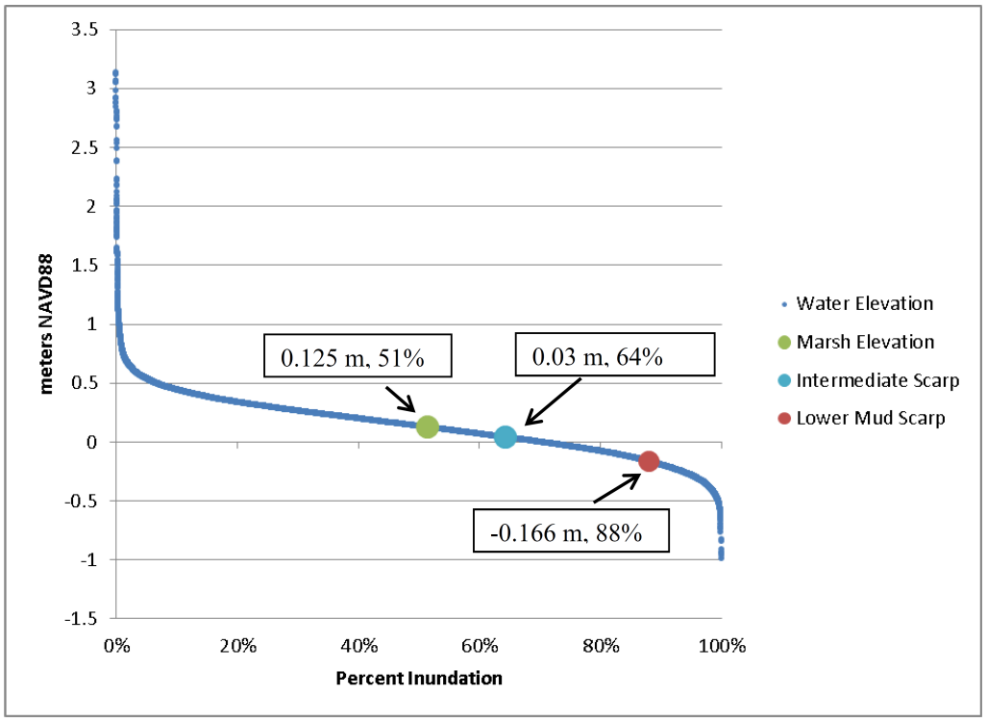

Figure 6 Stage duration curve for the study site. The cumulative frequency of each water-level is plotted versus water elevation showing the frequency of inundation of the lower mud scarp, the intermediate marsh scarp and the marsh platform from 2008 to 2012.

Meteorological observations during deployment period

Wind analysis for the two deployment periods December 14 to December 22, 2012, and December 22, 2012 to April 30, 2013 show similar patterns to the long term winter record (dominant wind direction from the north and northwest) (Figure 5). Three distinct frontal systems with differing characteristics moved through the study area during the deployment period (Figure 7); however the first system was not fully recorded in the data thus not used in the analysis. The second front (event 1) occurred on 12/18/2012 producing winds from the north at 4-6 m/s for approximately 8 hours (Figure 7). Although this was not an intense system, it was associated with a lower atmospheric pressure (10.1 dbar) and occurred at a higher tide (0.15 m NAVD88 or 0.316 m depth) when the marsh surface was inundated. The third system (event 2)

moved through the study site on 12/19/2012 and produced sustained winds from the NNW at 13-15 m/s with gusts up to 18-20 m/s for more than 24 hours. This event was associated with a high atmospheric pressure (10.32 dbar) that, when combined with the set down produced by the northwest wind and a falling tide, eventually suppressed the water elevation exposing the instruments (Figure 7). A difference of 1 millibar (Mb) in atmospheric pressure can cause a difference in sea level of about 0.01 m (Wunsch and Stammer, 1997; Singh and Aung, 2005). However, the rapid onset of persistent winds perpendicular to the coastline produced enough wind set up to inundate the marsh. This can be seen in Figure 7 b (Event 2) where an increase in northerly winds caused an abrupt increase in water level (up to 0.2 m) during a falling tide and remained above the predicted astronomical tide for 8 hours. Also note that increasing atmospheric pressure suppressed the water levels further (Figure 7b), despite a decline in wind intensity, for approximately 24 hours; this suggests that atmospheric pressure may play an important role in contributing to the water level variability at the site. This depression of the water surface under high atmospheric pressure, and its elevation under low atmospheric pressure, is often described as the inverted barometer effect (Wunsch and Stammer, 1997). Changes in sea level due to barometric pressure seldom exceed 30 cm (Singh and Aung, 2005), but this effect can be important as it is usually associated with wind set-up during the storm. This analysis will consist of the complete data from the latter 2 events and will be referred to as event 1 and event 2.

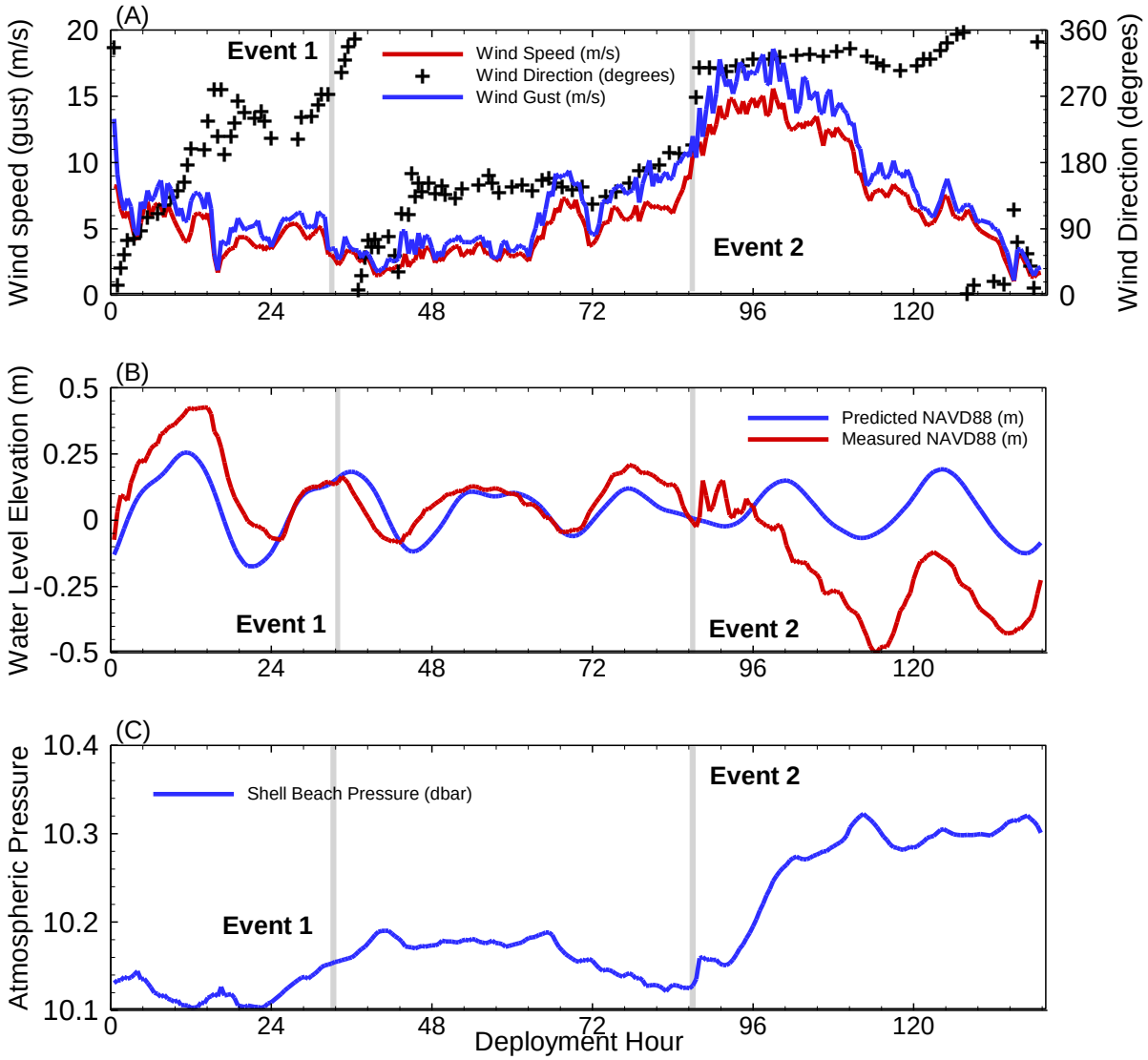

Figure 7 Meteorological data from NOAA station 8761305, Shell Beach, Louisiana during the deployment period of December 12/17/12 to 12/22/12. Frontal event are marked with vertical grey lines; a) Wind speed and direction, b) Observed and predicted water levels, c) Barometric pressure.

Examination of the water elevation data recorded by the instruments at the site shows the frequency and depth of inundation as well as the effect of winds and atmospheric pressure. The dashed lines in Figure 8b represent the elevation of the instrument (Vector ADV) deployed on the lower mud flat (black dashed line), and the instrument (RBR) deployed on the second intermediate marsh terrace (red dashed line). The solid lines in Figure 8b show the water surface

elevation at Shell Beach tidal station and the measured water surface elevation measured by each instrument. Figure 8 shows that the lower mud scarp remained submerged throughout the deployment period (red solid line) except late into the high pressure event (event 2). The instrument velocity probe was similarly inundated during each tidal cycle with exposure at low tide, while the second intermediate marsh scarp was inundated daily (blue solid line) with a maximum water elevation of 0.4 m NAVD88 during the highest tide or an equivalent 0.23 m of inundation

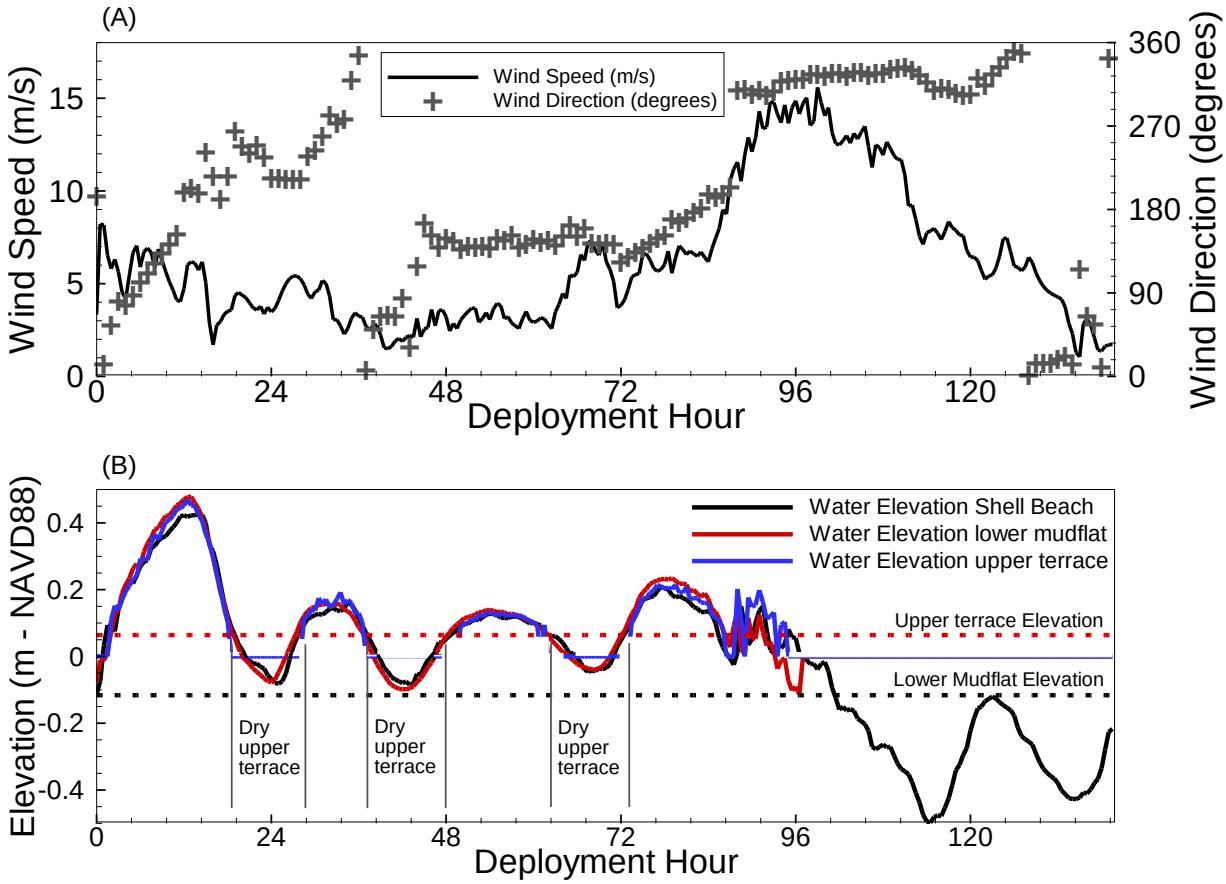

Figure 8 Wind speed and direction recorded at Shell Beach during deployment period 12/17/2012 to 12/22/2012 shown with water elevations recorded by the deployed instruments at the study site. Water surface elevations are shown with solid lines and dashed lines represent the elevation of each instrument located on the marsh. Locations are inundated when the water elevation exceeds the instrument elevation.

The two frontal systems represent two different scenarios that occurred with different wind speed and atmospheric pressure combinations (Figure 7). Event 1 was a higher water (larger tidal range), lower wind intensity, and lower atmospheric pressure event relative to event 2 which was a period of lower water, higher wind speed and higher atmospheric pressure. This can be seen in the measured data (Figure 8), where during Event 1 (deployment hour 36); relatively high water levels inundate the marsh platform (dashed red lines) allowing waves to reach the upper marsh platform. Event 2, (deployment hour 80 – 96), is marked by a decline in the water elevation due to falling tide and rising atmospheric pressure (Figure 7). During the second event the astronomical tide was decreasing (falling tide and lower range due to spring to neap variation) at the same time as a high pressure frontal system was approaching. An abrupt shift in the wind direction (south to northwest) and magnitude (~5 to 15 m/s) contributed to an increase in local water elevation due to wind and wave setup. Within several hours, the effects of atmospheric pressure and astronomical forcing on water levels became dominant over the wind effects, thus suppressing water level locally and facilitating wave attack to the lower mud scarp. This can be seen in Figure 7 and Figure 8, where an increase in wind speed forces an increase in water level while the astronomical tide was predicted to decrease, followed by a large increase in atmospheric pressure with corresponding decrease in water level to an elevation below the predicted astronomical tide.

Wave Analysis

Wave heights observed in Lake Borgne and the lower mud scarp from both events positively correlated with wind speed and wind direction, with the largest waves (~0.9 m) developing during strong northwest (12-15 m/s) winds during event 2 (Figure 7 and Figure 8). Figure 9 shows simultaneous observations measured at the offshore and nearshore locations.

This time series of wave heights demonstrates the effect of water level in controlling wave transmission by hindering wave growth and inducing wave breaking. Figure 9 shows an increase in wave height with the onset of northerly wind at both the offshore and nearshore locations. With persistent winds from a northerly direction, wave heights continued to grow at the offshore location (Figure 9); however deceasing water levels at the nearshore location (Figure 9) limit wave growth and force a decrease in wave height.

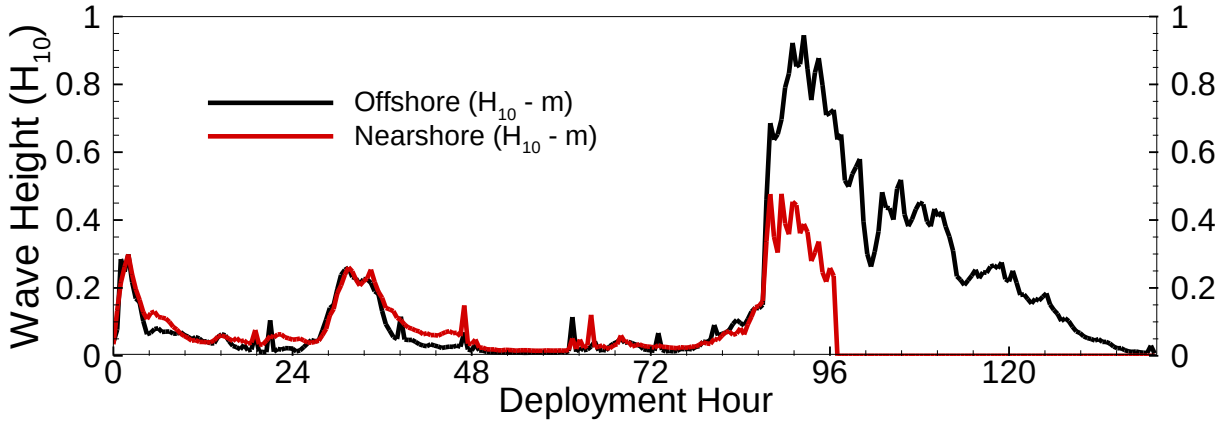

Figure 9 Measured waves heights at the offshore location (Ocean ADV) and at edge of lower mud scarp (Vector ADV) showing the effect of water level on nearshore wave development. The time series shows a rapid increase in wave height at both locations with increased wind speed from the north during event 2. Continued winds from the north increases wave heights offshore, however decreased water levels (Figure 7a and 8b) force a decrease in wave heights at the nearshore location. Winds continue from the north but decreasing intensity results in decreased offshore wave heights.

Computed wave characteristics from measurements at the lower mud scarp demonstrate that waves are very steep or are broken approximately 30% of the time during the deployment period. During event 1, 11% of the waves approaching the site were breaking while 91% of the waves were breaking during event 2. Figure 10 shows that the waves arriving at the lower mud scarp from both events are broken during peak conditions, and is supported further by calculation of the Iribarren Number, ξ_b (an indicator of the type of breaking wave) suggesting spilling and plunging type beakers. Values for ξ_b ranged from 0.5 - 1.1 for the broken waves (Table 4).

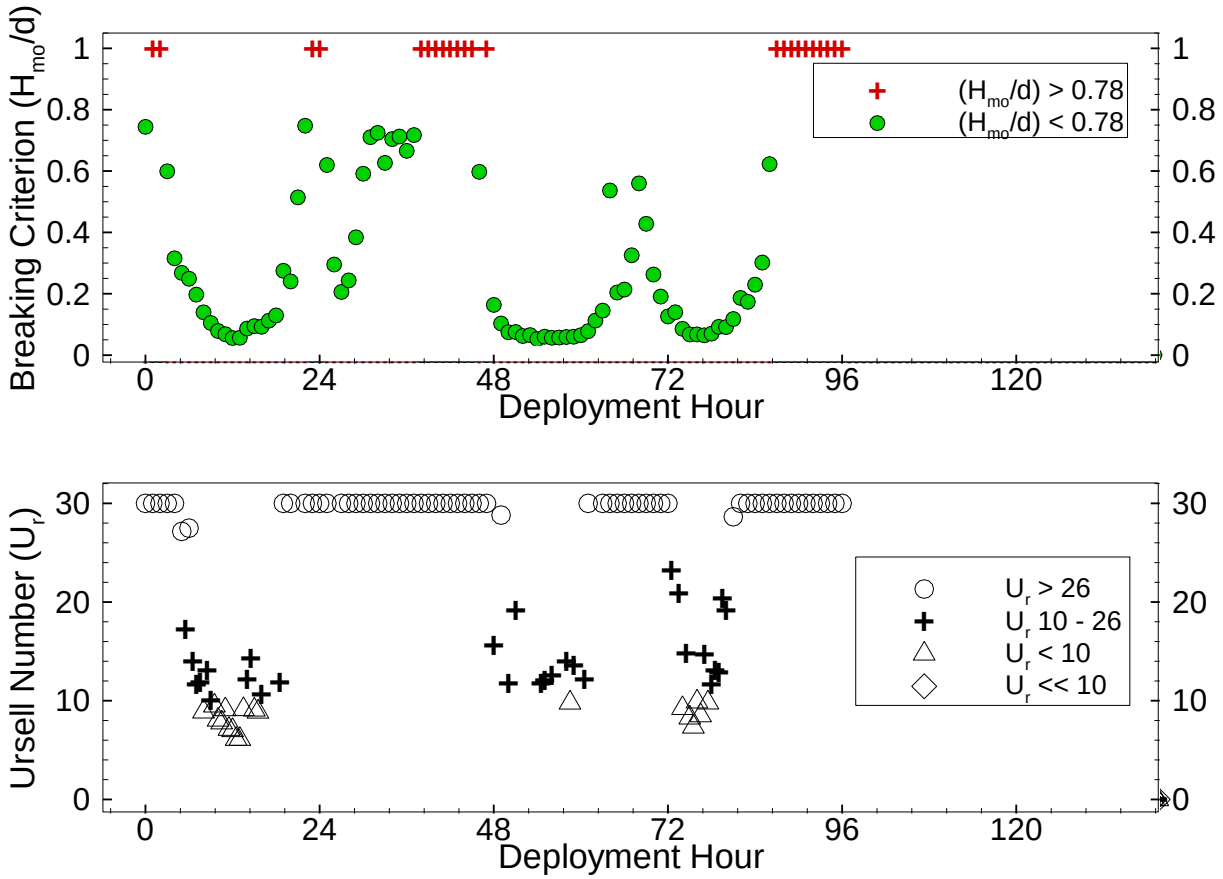

Figure 10 Wave characteristic at the lower mud scarp. Upper plot show the breaker index which is the ratio of wave height over water depth. Values greater the 0.78 indicate broken waves. Lower plot shows the Ursell number which is a measure of wave nonlinearity and demonstrates that the measured nearshore waves are highly nonlinear or broken as they approach the marsh edge.

Moreover, the unbroken waves arriving at the site (Figure 10) evaluated using the Ursell Number are highly nonlinear Stokes and Cnoidal waves. These data support the hypothesis that during winter storms, waves are short period, high amplitude, and are capable of transferring a greater amount of energy to the marsh edge than waves generated during fair weather conditions

Significant wave heights (H_{mo}) for event 1 in lake Borgne (0.14 m) were very similar to those arriving at the lower mud scarp (0.16 m). The same observations appear correct for all other wave characteristics such as average, maximum and the upper 10 percentile waves (H_{10},

Table 5). During event 2 however, a pronounced attenuation of waves (~30%) between the two sites (from 0.4 – 0.27 m) signifies the importance of inundation depth. The 95th percentile wave bottom velocities at the lower mud scarp had an average value of 0.15 m/s during the entire deployment period. Event specific velocities ranged from 0.23-0.45 m/s, (mean 0.32 m/s) during the first event and 0.53-0.87 m/s, (mean 0.73 m/s) for the second event. Detailed wave and velocity measurements and statistics for both events are presented in (Table 5).

Table 5 Standard wave parameters calculated during event 1 and event 2 at the offshore location (Lake Borgne) and the wave heights and velocities at the nearshore location (lower mud scarp).

	Event 1		Event 2	
	Lake Borgne	Lower Mud Scarp	Lake Borgne	Lower Mud Scarp
Water elevation (m NAVD88)		0.15		-0.05
Water depth (m NAVD 88)		0.32		0.12
Wave heights (m(std))				
H_{mo}	0.14 (0.03)	0.16 (0.04)	0.40 (0.05)	0.27 (0.03)
H_{mean}	0.09 (0.05)	0.11 (0.04)	0.25 (0.03)	0.18 (0.02)
H_{10}	0.18 (0.07)	0.2 (0.08)	0.49 (0.07)	0.35 (0.04)
H_{max}	0.40 (0.1)	0.39 (0.15)	1.30 (0.1)	0.77 (0.07)
Velocity (m/s(std))				
u_b mean magnitude	na	0.15 (0.02)	na	0.39 (0.08)
u_b 95	na	0.32 (0.05)	na	0.75 (0.14)

Short Term Erosion

Observations at the site revealed the shore consisted of a series of erosional scarps and terraces extending from the marsh surface approximately 20 m to a lower mudflat near MLLW (Figure 3, Figure 11). Each scarp and terrace eroded deeper into the substrate with the lowest terrace, composed of consolidated organic-rich mud without root material, ending at a final scarp that dropped off to 0.5 m below the surface at the most seaward limit of the shoreline. The lowest terrace extended towards the shore approximately 6.5 m to a second scarp approximately

20 cm in height. The second terrace was composed of predominately mud with small amounts of root material, extended 7 m then terminated at a third scarp approximately 10 cm in height. The third terrace was composed of mostly root material and extended approximately 6 m to the marsh edge. This marsh edge morphology was present in varying degrees along the coastline for 500 m in either direction (Figure 12).

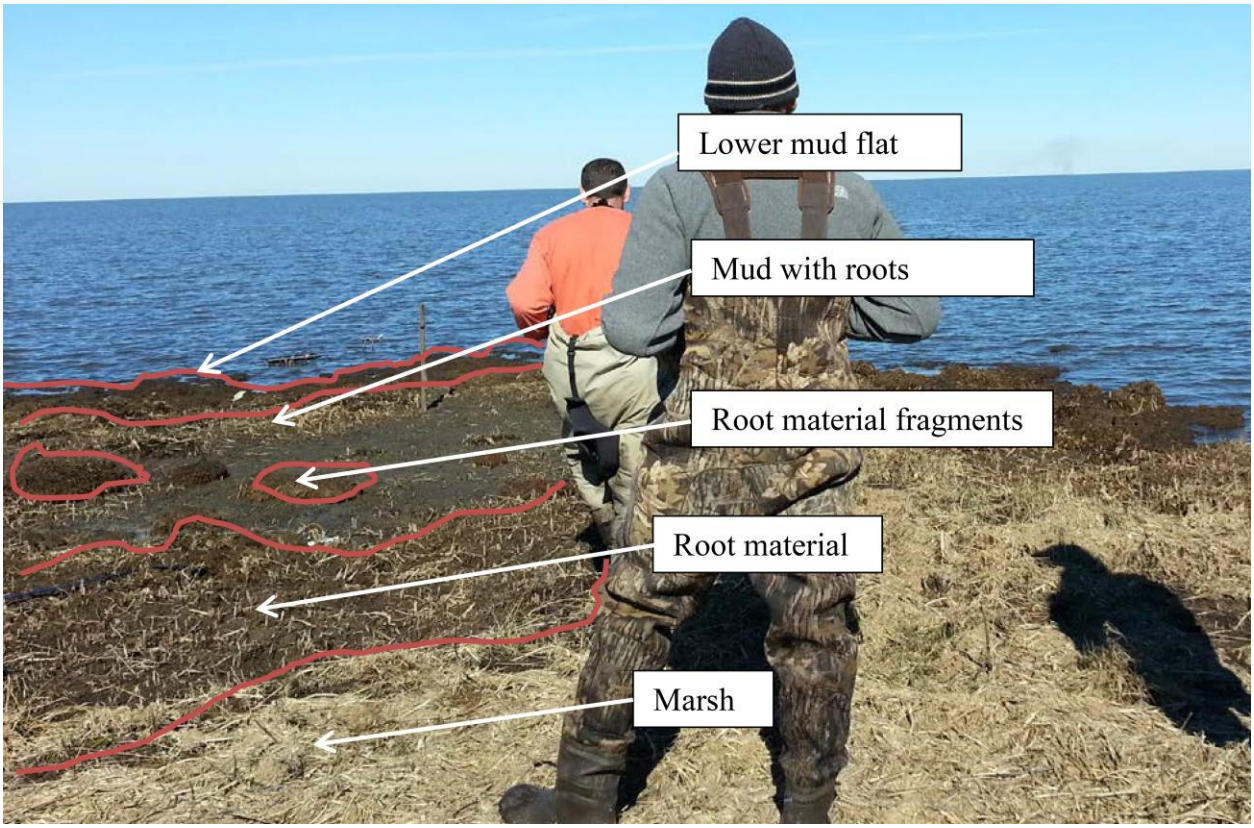

Figure 11 Image taken at study site on 12/22/12 during instrument recovery showing eroded lower mud flat, intermediate erosional scarps and terraces. Various sized fragments of sheared root material is noted

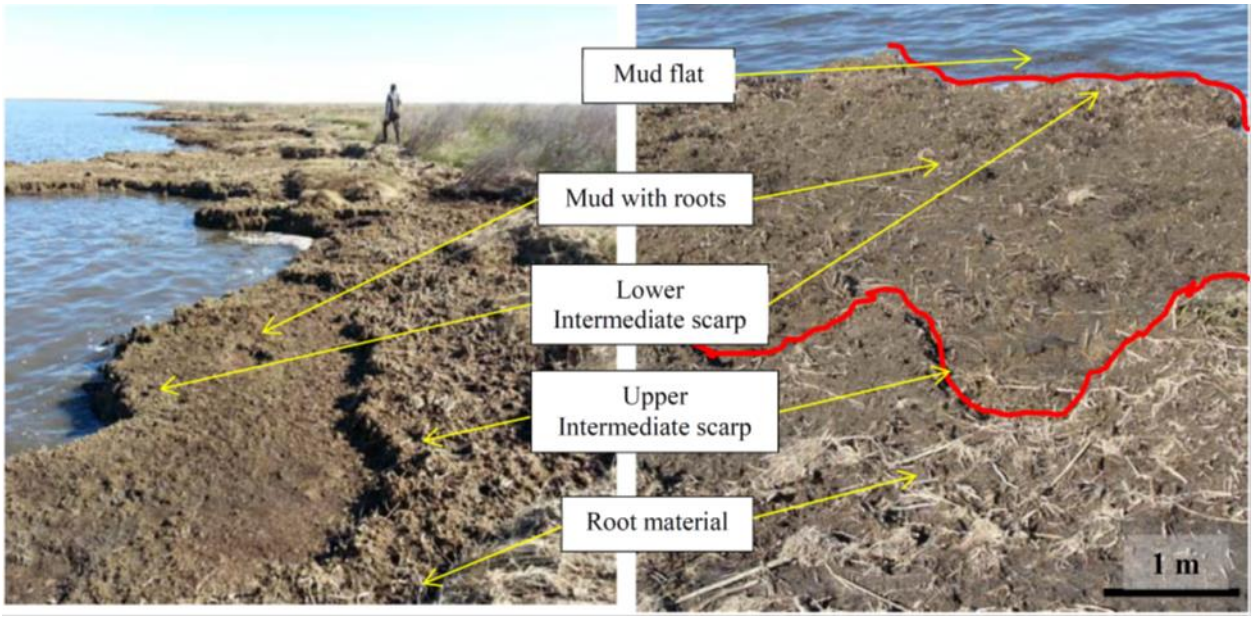

Figure 12 Images of study site on 12/22/12 during instrument recovery at several locations near transect showing varying degrees of erosion at the marsh edge.

On the preliminary visit in April 2012, small erosive scarps with terraces up to 1 m, 0.15-0.2 m below the water surface were identified on the marsh edge; however, there was no evidence of the large erosional features identified during the deployment in December 2012. It was determined that the large erosional features were not present on the preliminary visit thus developed between site visit 1 and 2.

On 12/22/2012 we recovered the deployed instruments and examined the study area. Erosion rates at the site were significant during the instrument deployment but impacted the marsh edge differentially. Erosion pin measurements on the platform (Figure 13) recorded an average of 0.026 m (n=8) of erosion over the eight day deployment (Table 6). More significantly, over the same period, the lower mud scarp receded at least 2.7 m with 0.2 m of material excavated from beneath the instrument located on the lower mud scarp (Figure 14, Figure 15).

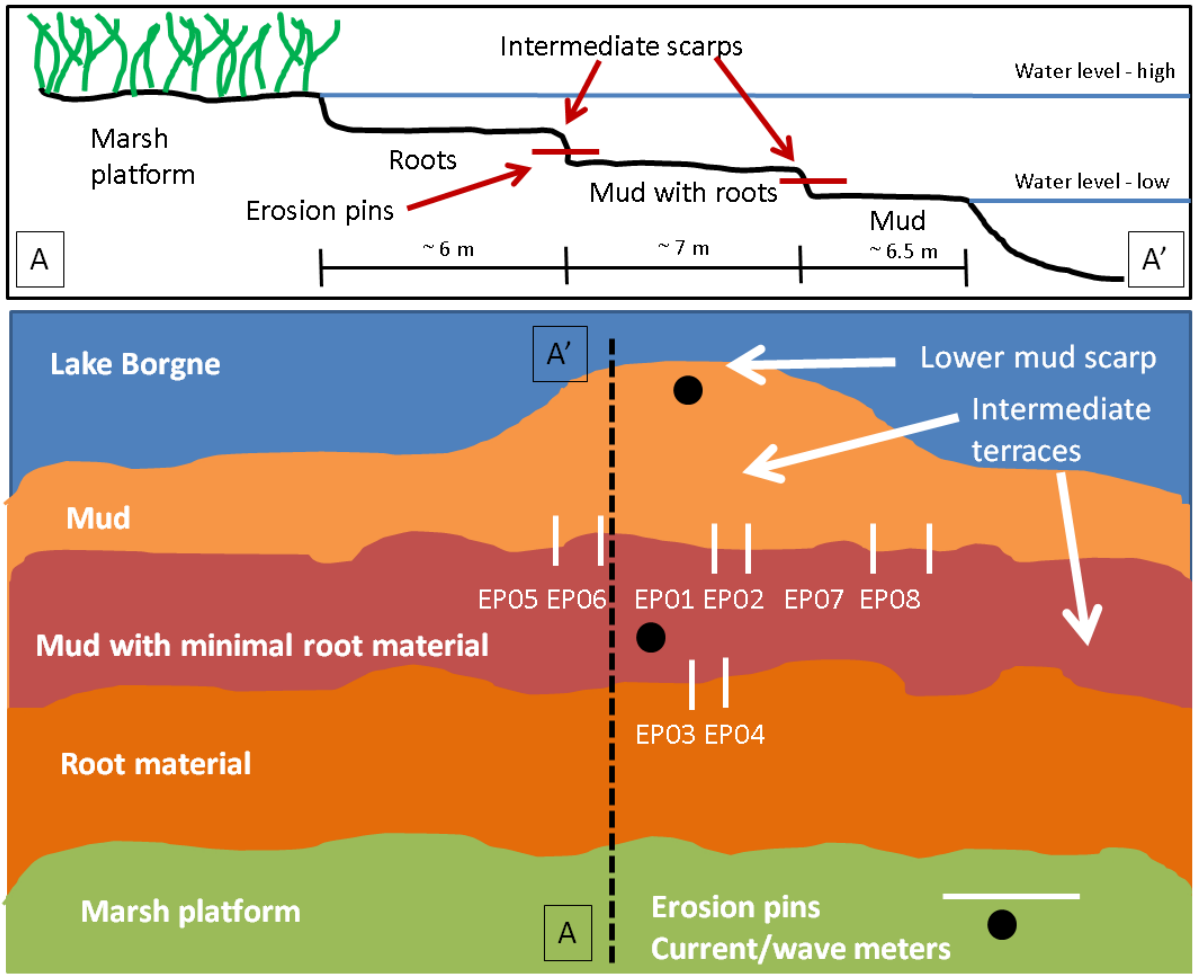

Figure 13 Plan view cartoon (bottom) of the study site outlining the intermediate terraces and lower mud flat, with a typical cross-sectional view (top) along A-A'. The white lines show the location of the 4 sets of erosion pins. The black circles show the location of the deployed instruments.

Table 6 Erosion pin measurements for each deployment period.

Site name	12/14/2012 to 12/22/2012 8 days	12/22/2012 to 04/30/2013 192 days
	Erosion m (myr-1)	Erosion (m) (myr-1)
EP01	0.030 (1.37)	
EP02	0.030 (1.37)	
EP03	0.025 (1.14)	1.5 (68.4)
EP04	0.030 (1.37)	1.5 (68.4)
EP05	0.015 (0.68)	
EP06	0.020 (0.91)	
EP07	0.050 (2.28)	
EP09	0.025 (1.14)	
Mean	0.026	
Std	0.006	
Lower mud scarp	2.7 (123.2)	

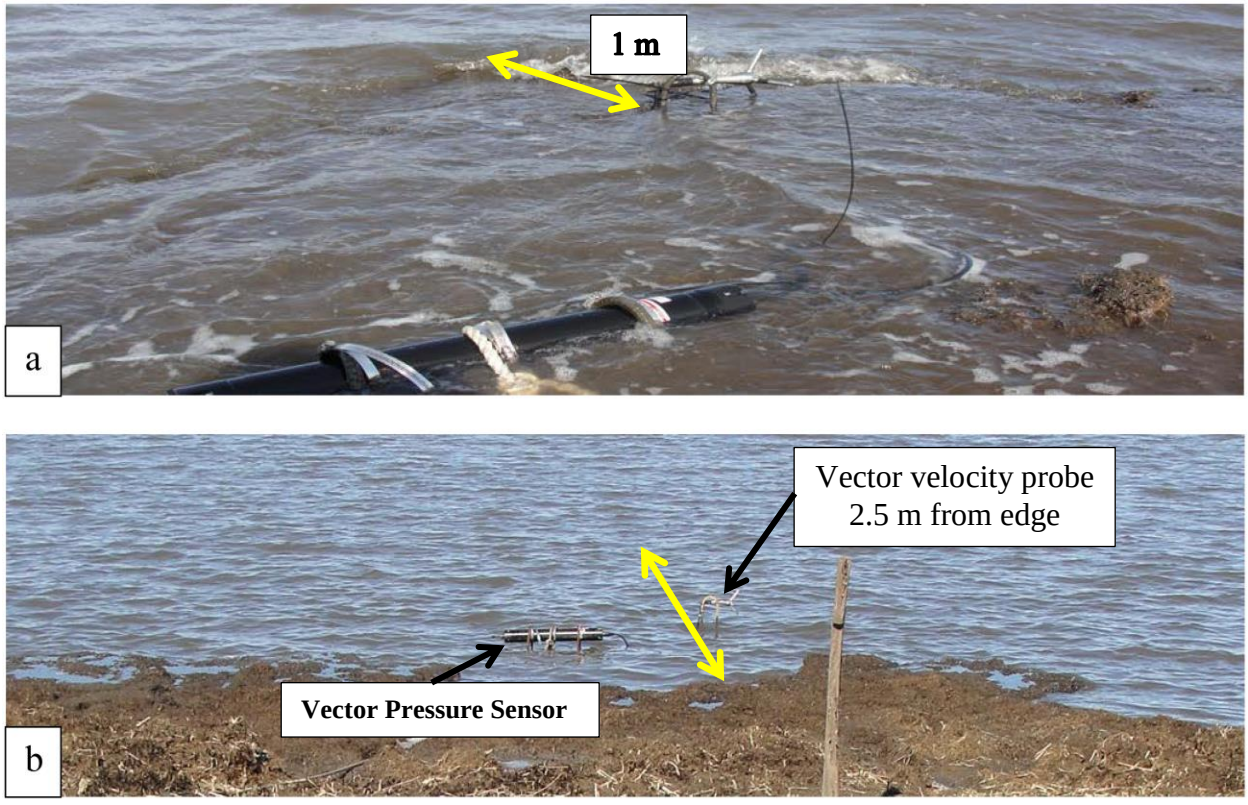

Figure 14 Vector ADV on the lower mudflat. a) Deployment - 12/14/2012 The velocity probe of the Vector ADV is mounted 1 m from the edge and 0.1 m above the lower mudflat while the Vector ADV pressure sensor is mounted on the surface of the mudflat; b). The Vector ADV shown during instrument recovery on 12/22/22012. The mud bank receded 2.5 m from its original position and 0.2 m of material was evacuated from beneath the pressure sensor.

Figure 15 Lower mud scarp on 12/22/2012. During deployment the mud platform extended 1 meter seaward of velocity probe. The photo shows the edge of platform 1.7 m landward of the velocity probe after event 2.

Various sized fragments of eroded root material were scattered across the platform ranging in size from 0.3-0.5 m (Figure 11). Approximately 0.02 m of muddy sediment was deposited over the intermediate scarp (RBR) partially burying the instrument. A heavy wrack line of mostly marsh stems and roots was located 25 m landward from the shoreline indicating the extent of inundation.

On the second field visit (4/30/2013) the lower mud scarp could not be accessed due to high water levels at the site and therefore the erosion along the lower profile could not be assessed with either erosion pins or topographic survey. However, the segment of the shoreline that could be measured shows the landward movement of the shoreline with a differential retreat of the scarps and a lowering of the erosional terraces (Figure 16).

Table 7 Marsh surface and instrument elevations.

Shoreline profile measurement locations	Elevation (m NAVD88)
Marsh platform (Edge)	0.154 (±0.03)
Intermediate marsh scarp (RBR Pressure gauge)	0.039 (±0.03)
Lower mudflat (Vector ADV Pressure sensor)	-0.166 (±0.06)

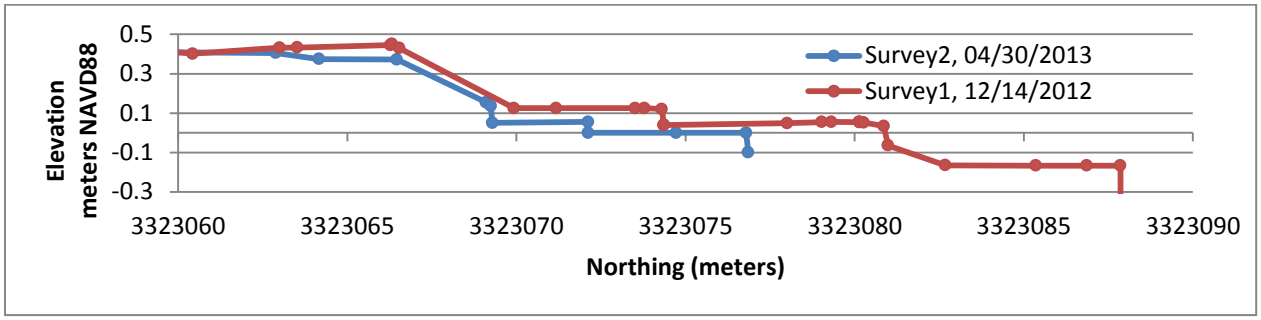

Figure 16 Cross shore profiles taken with DGPS on Survey 1 (12/14/2012 – red line) and Survey 2 (04/30/2013 – blue line) showing deflation and landward movement of profile.

During the second field visit the water elevation at the site was 0.154 m NAVD88 which is 0.115 m above the upper marsh scarp (RBR) elevation. Erosion pins EP03 and EP04 were the only pins recovered due to the elevated water level (Figure 13). The pins appeared to be fully eroded out of the marsh and were resting 1.5 m from the edge of a terrace made of mostly mud with some root material and covered by approximately 0.12 m of water (Figure 17). When initially placed, the pins were inserted 0.30 m into the upper intermediate scarps (Figure 17). The GPS coordinates for the pins and their orientation were unchanged (Figure 17). A distance from the scarp edge was taken using a tape measure, and added to the previously known insertion depth of the each pin. Despite the error introduced by using a measuring tape, (not greater than 10 cm), this provides for approximately 1.5 m of erosion at this scarp over 4 months.

Figure 17 Picture of submerged erosion pins EP03 and EP04 on 4/31/2012. Pins were in same orientation and location and appear to have been eroded from the marsh (2.5 m in 4 months).

Model Results

A numerical wave model was developed to study longer term wave climate predictions and to help in the predictions of marsh edge erosion at the site. Validated against observations, this forecasting tool can be valuable in estimating future marsh edge erosion trends, under future scenarios of climate change (ie. sea level rise, subsidence etc.). Although not the focus of this study, climate change could equally impact the elevation of the different marsh environments and the depth of the basin (ie Lake Borgne), both of which can impact wave climate and hence erosion rates. By correlating observations of incoming wave energy from Lake Borgne with measured nearshore wave heights (Figure 18), a 3rd degree regression function was developed to transform predicted offshore waves to the nearshore environment (Figure 18). This function required adjustment as the unadjusted function imposed an artificially lower wave height at the nearshore marsh environment. For example, note in Figure 9 that wave heights of 0.5 – 0.6 m were attenuated to approximately 0.2 m while wave height was still increasing offshore. This

artificial attenuation is due to the decreased water level during the second event, forcing a decrease in wave height at the nearshore location resulting in the divergence of the measured and predicted signals (Figure 9).

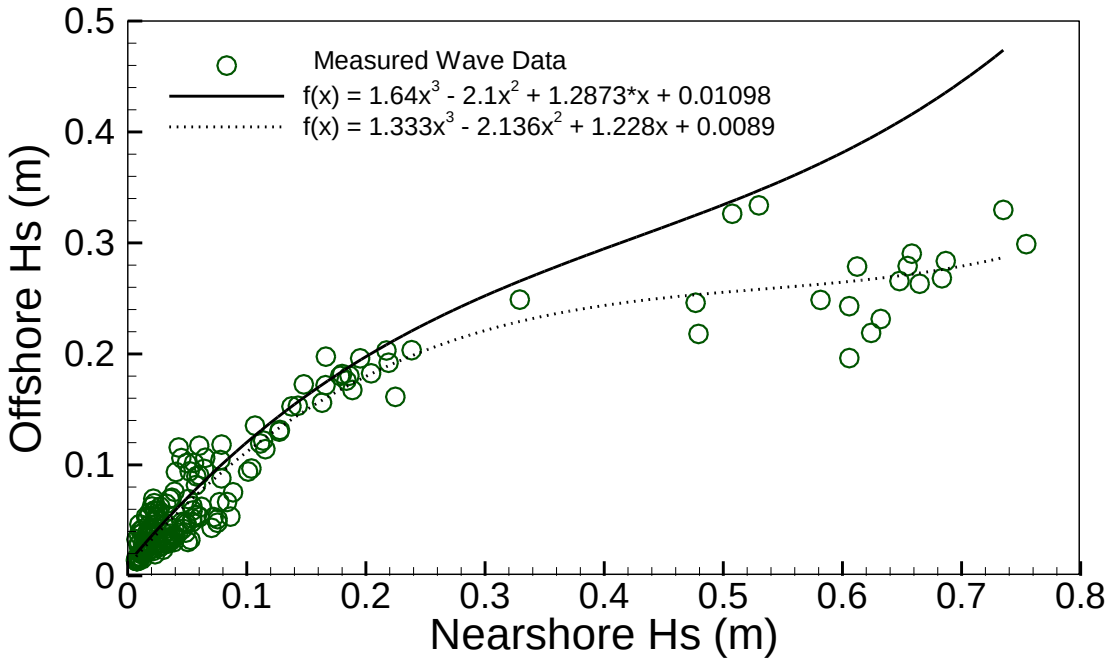

Figure 18 Plot of measured offshore waves (Ocean ADV) vs. nearshore waves (Vector ADV). Dashed line shows a trend line fitted to data without adjustment, while solid line shows the adjusted curve to prevent under-prediction of wave heights due to the decreased water level during the second event imposing an artificially lower wave height at the nearshore location.

Correlation of the observed and predicted wave height remained acceptable after the adjustment with a correlation coefficient of 0.86. This adjusted regression was then used for all future simulations to transform forecasted waves from the offshore to the marsh edge. The transformed waves were then used to calculate total and mean wave power and used in the erosion calculations.

Quantitative comparisons based on regression analyses and index of agreement were completed for the simulated waves against observations during the deployment period and are shown in (Table 8).

Table 8 Quantitative comparisons of observed and predicted wave heights.

	Observed wave heights		Predicted wave heights		Correlation coefficient	RMSE	Index of agreement
	Mean (m)	Std. dev. (m)	Mean (m)	Std. dev. (m)			
Offshore Waves	0.132	0.171	0.176	0.217	0.904	0.006	0.92
Transformed Offshore vs. Nearshore Waves	0.079	0.078	0.116	0.093	0.859	0.010	0.89
Wave Bottom Velocity	0.190	0.234	0.301	0.320	0.936	0.007	0.91

Measured and predicted offshore wave height show a high index of agreement and correlation coefficients with scores of 0.90 and 0.92. Results for the transformation of the offshore waves near the shoreline are slightly less at 0.85 and 0.89, suggesting that the regression function can effectively translate waves from the offshore to the marsh edge with 85 – 90% confidence. The lower scores are the result of the decreased wave heights forced by lower water levels during the second event as previously discussed. Regardless, this is a fairly good index of agreement and no further adjustments were performed, owing to the fact that the forecasting model was intended to be simple and allow for several years of wave simulations and resulting erosion.

Wave heights were calculated using methods described by Young and Verhagen (1996), using wind data collected at Shell Beach. The wind data was subsampled to select only the winds that occurred when the water level exceeded the elevation of the lower mud. The selected winds were then used to calculate waves, and were binned by wind direction into 15 degree directional bins. Waves generated from winds between 270° and 45° were then used to calculate

wave energy and wave power (see methods for details). A time series comparison between hourly observed and predicted wave heights during the deployment period is shown in Figure 19. Values for both offshore and nearshore predicted waves heights are listed in Table 9.

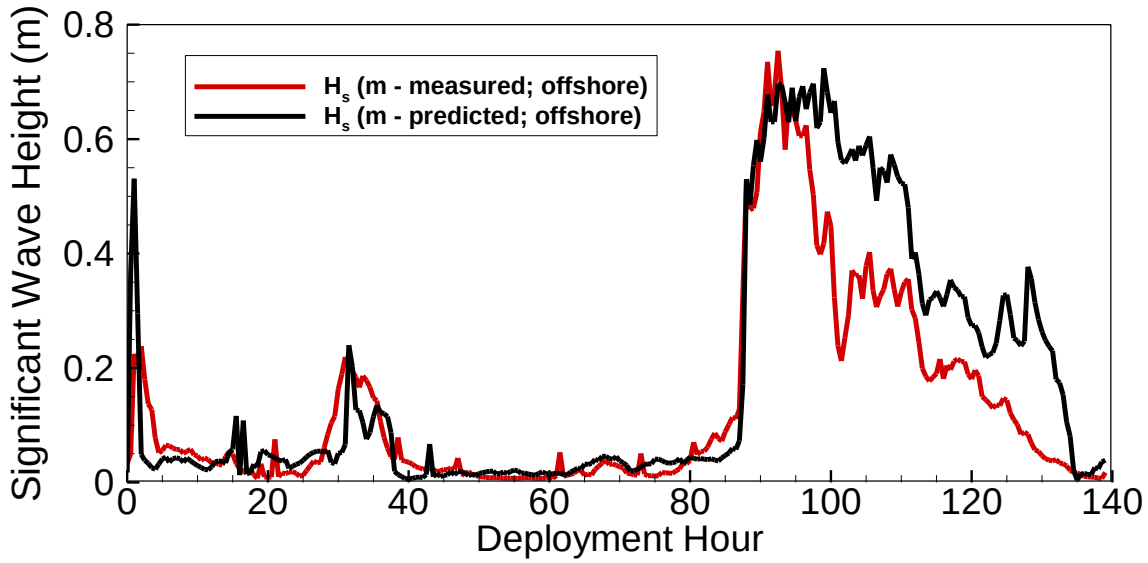

Figure 19 Time series of measured offshore wave heights (red) and predicted offshore wave heights (black) using methods described by Young and Verhagen (1996).

Table 9 Predicted wave heights for each annual and winter period.

Annual	Hs (m) Mean Offshore	Hs (m) Max Offshore	Hs (m) Mean Nearshore	Hs (m) Max Nearshore
2011	0.13	1.23	0.08	0.62
2010	0.15	1.7	0.08	0.89
2009	0.12	1.4	0.09	1.4
2008	0.13	1.7	0.1	0.63
Mean (m)	0.13		0.09	
Std. Dev. (m)	0.04		0.01	
Winter	Hs (m) Mean Offshore	Hs (m) Max Offshore	Hs (m) Mean Nearshore	Hs (m) Max Nearshore
2012	0.15	0.8	0.1	0.54
2011	0.13	1.3	0.09	1.1
2010	0.15	1.2	0.09	0.55
2009	0.2	2.3	0.13	1.3
2008	0.14	1.3	0.08	0.4
Mean (m)	0.16		0.09	
Std. Dev. (m)	0.02		0.02	

The calculated wave energy and wave power was used to predict the erosion rate at the site in m/y using previously discussed methods by Mariotti and Fagherazzi (2010). An erosion rate for the first

deployment period (8 days) was calculated by first using the measured wave heights to compute wave power (P) using Equation 22. Next, the critical wave power necessary to erode the marsh edge, (P_{cr}), was subtracted from the calculated wave power then the result was adjusted (by changing β) to generate a value for R that is approximately equal to the erosion measured at the site during the first deployment period. The erosion measured at the upper intermediate scarp, (3 cm over 8 days; 1.37 m/y equivalent for pins EP03 and EP04) was used instead of the erosion rate measured at the lower mud flat (2.7 m over 8 days; 123.2 m/y equivalent) as the former value is more representative of the documented erosion rates of 2.5 m/y (Watzke, 2004). Wave conditions were then predicted for the first deployment period using wind data following the methods of Young and Verhagen (1996). These predicted waves were first compared to the measured waves at the site, and then used to generate values for R to compare with the previously calculated erosion rates using the measured waves. The ratio of P/R using measure waves was compared to P/R using predicted waves and was within 0.1 standard deviations (Table 10). The procedure discussed above was used to find a value of β that would produce the erosion measured during the second deployment period (192 days) using the wave power from predicted waves during that period. The ratio P/R for the measured waves during deployment period 1 was also compared to the P/R for the predicted waves for deployment period 2 (no measured waves) and was within 0.06 standard deviations (Table 10). The value of β that was determined over the longer deployment was used to predict R for all future simulations; both annual as well as winter periods. Following Mariotti and Fagherazzi (2010), values for P_{cr} that ranged from 3 W to 15 W were used. These values correspond to the wave power produced by waves 7–15 cm (assuming wave group celerity of 0.5 m/s). Trenhaile (2009) used similar values

for erosion threshold values in a model for steeply sloping bluff retreat caused by broken wave impact forces.

Table 10 Predicted values for total wave energy (E), total wave power (P), mean wave power (Pmean) and erosion rates (R) for each annual and winter period considered.

	Hours (count)	E (kJ/m^2)	P (kW/m)	P_{mean} (kW/m)	R (m/y) (P_{cr}=15)	R (m/y) (P_{cr}=5)	R (m/y) (P_{cr}=3)
Observed	17	0.37	0.68	0.04	1.02	1.29	1.51
Predicted	17	0.32	0.58	0.03	0.95	1.28	1.55
				Mean	0.99	1.29	1.53
				Std. Dev.	0.05	0.01	0.03
Winter							
2012-13*	809	40.9	97.2	0.12	4.0	4.25	4.45
2011-12	661	31.6	77.4	0.16	5.6	5.83	6.02
2010-11	847	38.2	90.8	0.11	3.5	3.75	3.95
2009-10	1340	85.9	248.4	0.19	6.5	6.73	6.93
2008-09*	880	31.9	72.1	0.08	2.5	2.77	3.0
				Mean	5.20	5.44	5.63
				Std. Dev.	1.54	1.53	1.53
Annual							
2011	2084	82.1	197.8	0.09	3.0	3.29	3.49
2010	2424	110.9	261.0	0.10	3.1	3.35	3.55
2009	2415	133.9	365.2	0.15	5.2	5.43	5.63
2008*	1139	52.0	129.0	0.11	3.7	3.99	4.19
				Mean	3.77	4.02	4.22
				Std. Dev.	1.24	1.22	1.22
P obs / Ppred		1.15					
R obs/ Rpred		1.01					

*missing data; not included in mean

The results for wave energy, wave power, and the resulting erosion rate are listed in Table 10, grouped by season and year. The mean erosion rate (*R*), calculated with winds during the winter season, using values for P_{cr} of 3, 5 and 15 watts, ranged from 5.20 - 6.93 m/y (±1.4), while the mean erosion rate (*R*) using an annual wind record ranged from 3.77 - 5.63 m/y (±0.9). This variability in *R* can be expected since it is dependent on factors that vary annually and or

seasonally such as wind speed and direction, water depth, vegetation, root health, and marsh stratigraphy. Larger values of *R* during the winter season (5 months) compared to the remainder of the year (7 months) indicate that frontal systems contribute a larger proportion of the edge erosion experienced at the site (Table 10).

The predicted erosion rates (*R*), calculated with a P_{cr} of 5, were compared to 3 different published erosion rates that were calculated with field measurements or digitized shorelines (Table 11). We estimated that a value for P_{cr} of 5 would be the most appropriate for the wave power needed to erode the upper intermediate terrace at our site. The erosion rates from Penland et al. (2002) were calculated using digitized shorelines and were measured along a transect that was located within 500 m of the study site. Martinez et al. (2009) also used digitized shorelines and averaged erosion rates across segments of the of Lake Borgne shoreline; this study site was included in a 17 km segment of the Lake Borgne shoreline. Watzke (2004) recorded field measurements of marsh edge erosion from 1999-2003 in Terrebonne Bay. Additional shorelines were digitized in this study from aerial imagery (1989, 2007, and 2013) and used in combination with the Louisiana Barrier Island Comprehensive Monitoring Program (BICM) shorelines to re-analyze and re-calculate erosion rates at the location of the study site (Table 12). The predicted values for *R* are comparable to published long-term erosion rates at the site until the 1990's when rates increase significantly, especially 2004-2005 which is the period with Hurricanes Cindy, Katrina, and Rita. The predicted values for *R,* 4.02 (±1.2), are comparable to published erosion rates for the site of 5.8 m/y from 1930-1998 (Penland et al., 2002) and 5.6 m/y from 1930-1995 (Martinez et al., 2009) (Table 11). The predicted values for *R* appear to underestimate recent (1998-present) erosion rates at the site (17.6 m/y), however the measured rates are much closer (8.89 m/y) after omitting the 2004-2005 erosion (Table 12). However, *R* predictions

overestimate erosion rates when compared to field measurements of marsh edge erosion in Terrebonne Bay (2.5 m/y; Watzke, 2004) as well as historical rates at the site (2.9 m/y; Martinez et al., 2009,Table 11).

Table 11 Published erosion rates for Biloxi Marsh (Penland et al., 2002 and Martinez et al., 2009) and Terrebonne Bay (Watzke, 2004).

Penland etal., 2002		Watzke, 2004		Martinez et al., 2009	
Dates (y)	Rate (m/y)	Dates (y)	Rate (m/y)		Rate (m/y)
1898-1995 (97)	5.3			1852-2005	2.9
1930-1995 (65)	5.8			1933-2005	5.6
1960-1995 (35)	9.1				
		1999-2003 (4)	2.5	1996-2005	6.0
				2004-2005	26.9

Table 12 Re-analysis of erosion rates calculated from previously (BICM) and recently (this study) digitized shorelines showing the erosion rates at the study site for specified periods, the same periods with the effects of Hurricane Katrina removed and tropical

Period	BICM Rate (m/y)	BICM less Katrina Rate (m/y)	Hurricane
1930-1989 (59)	6.7	6.7	
1989-1998 (9)	6.3	6.3	
1998-2004 (6)	8.8	8.8	Georges, Ivan
2004-2005 (1)	62.3	8.0*	Cindy, Katrina
2005-2011 (6)	10.7	10.7	Gustav, Ida, TS Bonnie
2011-2013 (2)	10.5	10.5	Isaac
Mean	17.6	8.9	
Std. Dev.	22.0	1.5	

*average of 3 previous rates

Discussion

Meteorology and storm effects

Meteorological conditions are the chief driver of wave climate on the marsh edge at the study site. Wave regime correlated strongly with wind speed, direction and atmospheric conditions, suggesting that while the first two can aid in generating the waves and determining their direction, the latter (coupled with astronomical variations) governs where waves (large or small) arrive at the marsh edge, and when they do, controls their transformation and transmission onto the shore. The wind speed determines the amount of energy that can be transferred to the waves, while the wind direction determines the fetch, which dictates the distance, thus length of time, that energy the can be transferred to the wave. Wind set up alters the local water level which controls wave growth and decay by controlling the local water depth. In addition to wind effects, atmospheric conditions during cold fronts also significantly influence water levels which determine the location on the shoreline where waves can attack. A difference of 10 dbar in atmospheric pressure can result in approximately a 0.1 m change in sea level. This suggests that the passing of a high pressure system can suppress water levels such that wave attack and erosion is focused on the lower scarps, whereas a low pressure system can elevate water levels such that for the same wind speed and direction, the marsh platform is now attacked and eroded. These effects are more important when considered along with wind and wave set-up, further modulating water level fluctuations during winter storms. This observation is in line with modeling results of Tonelli et al. (2010), where they demonstrated that wave thrust focuses wave energy dissipation at different elevations during fluctuating water levels. During observations at the site, this is documented where event 1 exhibits waves that are nearly fully transmitted (no decrease in wave height), at the lower marsh scarp suggesting that these waves are likely

impacting the marsh platform and intermediate or upper marsh scarps. In contrast to event 2 (Figure 8), the energy transmitted is initially focused to the upper scarp and terraces; but within hours is limited to the lower mud scarp, facilitating rapid meter scale erosion (Table 11 and Figure 15).

The temporal frequency as well as the duration of winter storms also plays an important role in the distribution of the total wave energy arriving at the marsh edge. This is seen very well during event 2 where the prolonged suppression of the water level concentrated the incoming offshore wave energy (H_{10} - 0.4-0.9 m) at the level of the lower sharp for nearly 24 hours.

Model Predictions for Marsh Edge Erosion

When comparing measured erosion rates to mean wave power (*R* versus *P*), the model results are in good agreement with similar studies in the Venice Lagoon, Italy (Marani et al., 2011) which implies a linear relationship between edge erosion (*R*) and wave power (*P*), and likely similar marsh stratigraphy (Figure 20). The scatter in their results is the product of assessing multiple locations and different observation periods. Our predictions are based on an average erosion rate at one location, therefore an increase or decrease in *P* would have a linear effect on *R*, however the slope similarity (0.035 vs. 0.029) reinforces further the site similarity and the proportionality of edge erosion to wave power. Moreover, our predicted values for *P* and *R* are generally higher than Marani et al. (2011) despite a similar trend. This can be explained in that Marani et al. (2011) describe sites with a single scarped edge and examined the forces affecting the scarp alone; therefore, water levels above the marsh surface were excluded, effectively decreasing the total energy arriving at the site. Although a reasonable approach, excluding submergence events is equivalent to ignoring erosion of the marsh surface during

those events from non-breaking waves. During submergence, while scarp erosion is minimal due to the absence of breaking waves, surface erosion is still possible due to shear produced by the wave orbital velocity at the marsh surface.

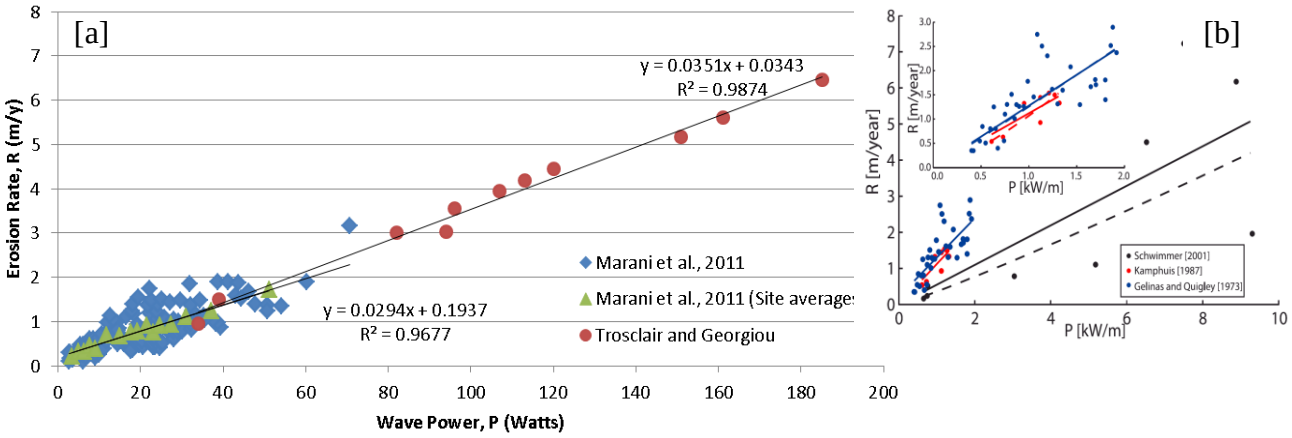

Figure 20 Marsh-edge erosion rates for the Biloxi Marsh, LA [a] compared to Marani et al., (2011) in the Venice lagoon, showing good linear correlation between edge retreat and wave power. Insert [b] shows results from other studies by Schwimmer (2001) and Kamphuis (1987).

When multiple scarps exist, such as the site herein, subjected further to different submergence regimes due to water level fluctuations, a hybrid approach to the marsh edge erosion model is needed. A better method would be to treat each scarp or terrace separately, applying a separate break or shear term based on water level. Waves approaching the site can be binned based on water level, such that the wave power is distributed among the scarps and terraces as shear or impact forces. This can better characterize local conditions and help establish a framework where different values for β and P_{cr} can be used, that better characterize each terrace and scarp, accounting for the differential erosion rates observed at the study site. The total erosion rate (R) would then be the sum of individual R for each terrace and scarp and could be written as follows:

$$R_T = \sum_{i=1}^{n} (R^i{}_{break} + R^i{}_{shear}) \quad (26)$$

where R_{break} is the erosion to the scarp face due to wave impact forces and R_{shear} is the erosion to the terrace surface due to wave shear stresses once inundated (for n number of scarps/terraces).

The predicted values for edge erosion rates (R; long-term) were very similar to long term rates measured at the site using digitized shorelines (Martinez et al., 2009; Penland et al., 2002). However, when predictions are compared to near term rates, they slightly underestimate erosion rates (Table 11). This can be attributed in part to the method used to calculate mean wave power. Since wave power is calculated from seasonal and annual records, by selecting waves within a specified direction (270 – 45 degrees), it may inadvertently exclude waves that arrive at the site at oblique angles. Omitting these waves is not critical for smaller storms, however, when they occur during tropical storms the waves can be effectively transmitted onto the marsh platform and contribute to surface erosion by shear produced on the terrace, or scarp erosion by energy release during rapid transformation (refraction/shoaling/breaking). For instance, a 1 m storm surge produced by tropical storms could increase the Lake depth to nearly 3.5 m, as well as inundate the terraces by 0.75 m. This condition may facilitate breaking conditions at the marsh platform, but little erosion due to breaking at the lower mud scarp. The recent increase in frequency and magnitude of tropical storms (Poore et al., 2009) has likely contributed to the increased erosion reported in the near-term rates by Penland et al. (2002) and Martinez et al. (2009). Examination of the near-term and longer-term erosion clearly shows that the longer the record, the lower the erosion rates appear. The lower erosion rate for the long-term record are likely the result of fewer named storms impacting the site (within 200 km), compared to recent years (16 hurricanes from 1930-1997 (0.24/y) versus 7 hurricanes from 1997-2013 (0.44/y))

(Poore et al., 2009; http://www.csc.noaa.gov/hurricanes/#). In addition, the increased magnitude of recent storms, for example Ivan, Katrina, Gustav and Ike has increased the near-term erosion rates (Barras et al, 2008; Couvillion et al., 2011). Watzke (2004) measured short term erosion rates (1999-2003) in Terrebonne Bay noting that during periods with tropical storm activity, 70% more erosion occurred.

Additional discrepancies in the predictions of short term erosion may be the result of grouping the effects of vegetation, sediment characteristics and marsh morphology into the β parameter. Short term changes in vegetation characteristics that may affect the vegetation's ability to resist erosion, such as seasonal variation or compromise after large storm impacts, is not captured in a time-average value of beta. This seasonal or annual variability is averaged across longer time intervals therefore does not have a significant influence on the long-term rates. The normalizing of transient effects with time allows a single value for β to produce reasonable results over longer time scales. Additionally, the value for P_{cr} (critical wave power for erosion) changes with substrate strength which varies with depth (Howes et al., 2010; Marani et al., 2013) and presence of vegetation (Day et al., 1994; Francalanci et al., 2013). The multiple wave cut terraces at the study site, each eroding successively deeper into the substrate, suggest multiple values of P_{cr} are needed to better characterize the marsh edge resistance to erosion at the study site. Moreover, water level dictates the primary erosive forces applied to the marsh edge, with shear dominating the terraced surfaces and impact/breaking forces dominating the intermediate scarps, each affecting different properties of the substrate, necessitating different values for P_{cr} to adequately characterize the marsh edge. Finally, although effects of nonlinear waves were included in the wave prediction methods (Young and Verhagen, 1996), as well as in the transfer function, some assumptions needed for the analysis were based on linear wave

theory. Since nonlinear waves transfer more energy than linear waves during transformation, the results would be biased towards under-predicting the amount of wave energy thus yielding generally a lower erosion rate.

Marsh edge erosion trends

H1 - Short period, high amplitude wind waves generated during cold fronts transfer a greater amount of energy to the marsh edge than waves generated during fair weather conditions. Measured wave characteristics support this hypothesis by showing the waves approaching the site are in fact high order nonlinear waves (Figure 10). During event 2, 91% of the waves were breaking at the shoreline, and combined with event 1, generated 80% of the total wave energy at the site during observations.

H2 - The energy transferred to the marsh edge during winter storms accounts for a greater proportion of the observed shoreline erosion compared to erosion rates produced during fair weather conditions. This hypothesis is supported by the model results as the predicted values of *R* (erosion rate) are greater during the 5 months of the cold front season (~5.44 m/y) than for the entire year (~4.02 m/y) (Table 11). Since mean wave power is proportional to the erosion rate, a reduction in the annual rate compared to that of the winter storm season indicates that the average wave power generated is higher during the winter season (with the exception of large storms). For example, if the erosion rate for the annual period (~4.02 m/y) is less than the erosion rate for the cold front season (~5.44 m/y), then summer erosion must be significantly lower. Increased winter erosion rates were also documented in Terrebonne Bay at 0.77 m/y, which is more than two times greater than summer erosion rates of 0.31 m/y (Watzke, 2004).

In addition, published long-term erosion rates are often inferred by examining shoreline change maps over temporal scales that include seasonal variations and post storm effect that may contribute to significant errors in identifying the location of the shoreline. Documented erosion rates that include intervals of large tropical storms are often characterized as purely event driven. While the importance of post storm events such as winter storms is acknowledged as a potential mechanism in the continued erosion of the shoreline, they are not fully explored as a significant erosion process. For example, storm effects such as marsh surface denudation and increase in salinity and sulfides cause excessive plant stress and can contribute to future wetland losses (Barras, 2007; Steyer et al., 2010). This secondary loss of wetlands is incorporated into the erosion rates calculated from data sets that span multiple years and do not distinguish between causes of erosion during these periods, which can underestimate the significance of winter storms in this process. Ultimately, however, the loss is through marsh edge erosion and waves are still the chief driver.

Formation of scarp

The regression of the marsh is associated with a steepening of the cross shore profile, which eventually leads to scarp formation (Schwimmer and Pizzuto, 2000; Schwimmer, 2001). Increases in water depth results in increased wave power reaching the marsh edge (Schwimmer and Pizzuto, 2000; Tonelli et al., 2010). For a given wave forcing, scarp erosion is a discontinuous process, with periods of surface erosion alternating with scarp failure and mass wasting (Allen, 1990; Schwimmer, 2001; Mariotti and Fagherazzi, 2010; Francalanci, 2013). Bank retreat was recently shown through numerical modeling and laboratory studies to be the result of wind waves weakening the substrate by triggering the formation of overhang profiles that slump during subsequent wave attack (Mariotti and Fagherazzi, 2010; Francalanci et al.,

2013). The presence of vegetation helps resist this process by delaying mass failures and maintaining the scarp profile (Day et al., 1994; Francalanci, 2013; Pant, 2013).

Wilson and Allison (2008) proposed an equilibrium profile for eroding marsh edges in southeast Louisiana which includes the lateral incision and retreat of the marsh surface forming a marsh scarp and an erosional surface that extends seaward until reaching a depth below local wave base (1.0 - 1.5 m depending on adjacent bay size and depth). The profile was described as erosion dominated with retreat rates at 1 m/y and was widespread throughout Breton Sound and Barataria Bay marshes. The preliminary visit to our site in April 2012 demonstrated this general morphology with the addition of small erosive scarps at the marsh edge with terraces up to 1 meter submerged by approximately 0.15-0.2 m during high water. However when we returned to the site in December 2012 it was apparent that a large event had negatively impacted the site as the marsh edge now consisted of a broad platform approximately 25 m wide with multiple wave cut terraces extending from the marsh surface to the lower scarp of organic rich mud. This likely represents a disruption in the equilibrium marsh edge profile with a shift toward an equilibrium state.

Mechanism of Retreat

Wave impact forces cause failure of the marsh edge by exerting unsteady normal forces to the scarp and shear stress on the terraces (Francalanci, 2013; Tonelli et al., 2010). As previously discussed, water levels have a significant effect on how wave forces focus energy on the scarp. An increase in water level allows larger waves to approach the marsh edge. Once transformed near the edge, these waves are highly nonlinear and apply large impact forces to the scarp as they break. During decreased water levels wave height growth is limited by water

depth; in the meantime, offshore wave heights are not appreciably affected. Thus during low water conditions large waves approach the lower mud scarp, transform rapidly, and then break delivering concentrated energy to the lower scarp.

Changes in water levels also control shear stresses contributed by waves. In general, increase in water depth decreases bottom shear stresses, however higher water levels inundate upper and intermediate terraces, thus promoting erosion not only by wave impact but also by bottom shear stresses produced by wave orbits. Vegetation has the effect of protecting the marsh surface from wave erosion (Mariotti and Fagherazzi, 2010); however the already severely impacted marsh edge at our site could not resist these forces. As the marsh root mats decay, soil shear strengths decrease appreciably allowing for physical processes to remove surface soils quickly (Day et al., 1994). At low water levels, bottom shear stresses produced by waves increase and promote the removal of previously eroded material below the lower scarp, thus maintaining the local water depth allowing the continued support of large wave during high water events.

The consistent passing of frontal systems at different water levels focuses wave forces to different locations along the marsh resulting in the differential erosion that changes the profile from a scarped edge to the multiple stepped terraces identified at the site. Removal of the protective effects of the vegetation by decomposition and/or erosion exposes the less resistant material to the erosive forces of the waves resulting in very high rates of erosion. The rapid erosion measured at the lower mud scarp (2.8 m over 8 days) must be indicative of a transient self-organization toward an equilibrium state. We suspect that larger events, such as the passing of Hurricane Isaac on August 29, 2012 may have impacted the site leaving the marsh surface denuded. Denudation is common in intermediate, brackish, and salt marshes after large storms,

and can range in width from 2 m to 13 km (Barras, 2007; Barras et al., 2010). Large areas of denuded marsh were found in Breton Sound after Hurricane Katrina (Barras, 2007). Also, the USGS reported significant damage to the marshes east of the Mississippi River in coastal Louisiana associated with Hurricane Isaac; however detailed information on location and extent of the damage could not be found (http://www.usgs.gov/newsroom/article.asp?ID=3398). This is further supported with data from the Shell Beach Station recording winds trending from the N to NE at 10-25 m/s for greater than 24 hours while the site was inundated by water levels 0.5-1m. These conditions could have produced sufficiently large waves to damage the site. Winds increased to near 30 m/s from the E to SE with water levels in excess of 3 m. Denuded marshes can partly or completely recover in one growing season if the root mat is not entirely destroyed (Chabreck and Palmisano, 1973; Chamberlain, 1959); however a few centimeters of additional surface erosion can prevent recovery (Morton and Barras, 2011). The subsequent passing of repeated frontal systems at our site, before the marsh could recover, differentially eroded the damaged marsh surface exposing the less resistant substrate. This facilitated further erosion at the marsh edge to produce the high erosion rates measured at the site. These accelerated rates can be expected to continue until a new equilibrium is met. While results of this process are not clear or available in the literature, there is an underlying process unidentified. This can be expected with the temporal and spatial uncertainty and variability of digital shorelines thus making it difficult to discern the processes involved in short-term shoreline change.

Models of Marsh Scarp Retreat

Wilson and Alison (2008) assumed a constant (and uniform) rate of lateral retreat in their conceptual model and recognized the potential influence of episodic winter and tropical storms as a method of shoreline retreat however; they do not describe how these events would disrupt

the profile. We provide results herein that help describe the mechanism by which significant marsh edge erosion occurs during a frontal season following a significant impact to the marsh shoreline. This process supplements the Wilson and Allison (2008) conceptual model by describing a method of scarp edge development and evolution. Although the exact mechanism by which the profile was disrupted is unknown, the return to an equilibrium (state) profile can be described through field observations as follows (Figure 21):

a) Begins with equilibrium profile for eroding marsh edges in southeast Louisiana
b) The marsh edge is compromised by events that weaken or remove the vegetation near the edge.
c) Repeated attack throughout the winter season by fontal systems with combinations of varying wind intensity, direction and water level.
d) A series of scarps and terraces form as a result of differential erosion due to differences in substrate resistance and wave attack at various water levels.
e) Decay and removal of marsh root material decreases the edge's resistance to further wave attack resulting in rapid retreat.
f) Finally, a new equilibrium is reached, or at least it is sought, pending the next storm event, as these are dis-equilibrium landscapes.

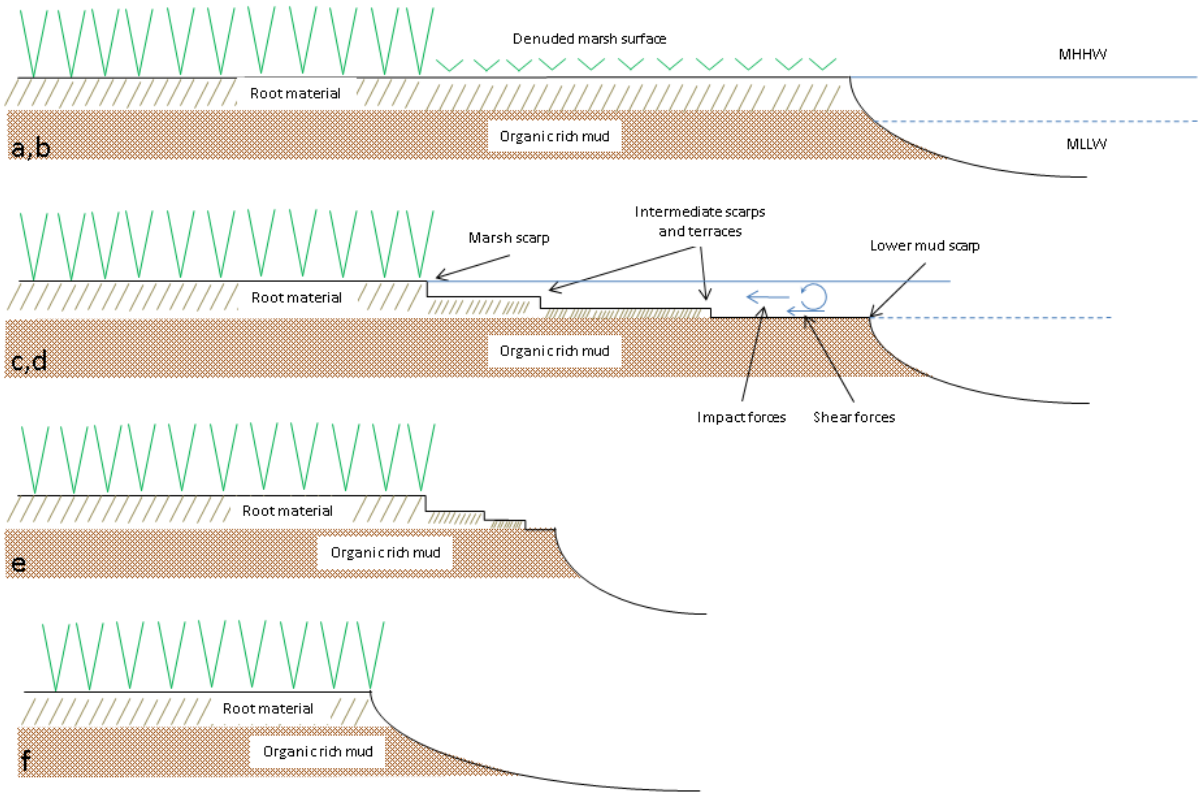

Figure 21 Method of scarp edge development and evolution showing mechanism by which significant marsh edge erosion occurs during a frontal season following a significant impact to the marsh shoreline. See description in text for items a-f.

Conclusions

Meteorological conditions such as wind direction and intensity and atmospheric pressure gradients are the chief driver of wave climate and water depth at the site. Water levels have a significant effect on how wave forces shape the shoreline by controlling the location where waves can attack and by determining the type of wave forces (shear vs. impact) that will dominate the erosion process. This control imposed by water level resulted in the differential erosion observed at our site. Increased water levels inundate the intermediate terraces which supports larger waves that eroded the marsh edge by both wave impact forces and bottom shear stresses. Decrease water levels limits wave from reaching the upper platform thus focusing wave impact forces on the lower scarp. Bottom shear stresses increase and promote the removal of eroded material from below the lower scarp maintaining the water depth.

The method used to implement the edge erosion submodel use to predict erosion at the marsh edge (R), gave reasonable estimates for long term erosion rates (4.02 ±1.2 m/y) compared to calculated long-term rates at our site (5.3 m/y) using re-analysis of digital shorelines developed by Penland et a. (2002) and Martinez et al. (2009) supplemented further by digitizing additional shorelines for more recent years. The predicted value of R underestimates near-term erosion rates which we attribute to the increased frequency and magnitude of tropical storms as well as the need for more appropriate values of β and P_{cr} to characterize the marsh edge stratigraphy.

High rates of erosion measured at the site (2.8 m lower mud scarp and 1.5 m intermediate scarp) suggest a transient self-organization toward an equilibrium state. Disturbance to the marsh edge, possibly due to the passing of Hurricane Isaac on August 29, 2013 may have destabilized the edge by eroding and denuding the marsh surface. Without the protective effects

of the vegetation, the shoreline is more susceptible to repeated wave attack during frontal storms. Wave forces cause the failure of the scarp by exerting intermittent normal and shear stress on the soil, at a location determined by water level, creating multiple erosive scarps and terraces thus imposing a non-equilibrium condition. The subsequent passing of repeated frontal systems, before marsh recovery, differentially erodes the damaged marsh surface exposing the less resistant substrate thus facilitating further erosion and producing the high erosion rates measured at the site. These accelerated rates can be expected to continue until a new equilibrium is met.

References

Allen, J. R. L. (1989). Evolution of salt-marsh cliffs in muddy and sandy systems: A qualitative comparison of British West-Coast estuaries. Earth Surface Processes and Landforms, 14(1), 85-92.

Smith, J. M., Cialone, M. A., Wamsley, T. V., & McAlpin, T. O. (2010). Potential impact of sea level rise on coastal surges in southeast Louisiana. Ocean Engineering, 37(1), 37-47.Asano, T., Deguchi, H., & Kobayashi, N., (1992), Interactions between water waves and vegetation: Proceedings of the 23rd International Conference on Coastal Engineering, ASCE, p. 2710-2723.

Ashton, A. D., Murray, A. B., Littlewood, R., Lewis, D. A., & Hong, P. (2009). Fetch-limited self-organization of elongate water bodies. Geology, 37(2), 187-190.

Augustin, L. N., Irish, J. L., & Lynett, P. (2009). Laboratory and numerical studies of wave damping by emergent and near-emergent wetland vegetation. Coastal Engineering, 56(3), 332-340.

Barbier, E. B., Koch, E. W., Silliman, B. R., Hacker, S. D., Wolanski, E., Primavera, J., ... & Reed, D. J. (2008). Coastal ecosystem-based management with nonlinear ecological functions and values. science, 319(5861), 321-323.

Barbier, E. B., Georgiou, I. Y., Enchelmeyer, B., & Reed, D. J. (2013). The Value of Wetlands in Protecting Southeast Louisiana from Hurricane Storm Surges. PloS one, 8(3), e58715.

Barras, J., Beville, S., Britsch, D., Hartley, S., Hawes, S., Johnston, J., ... & Suhayda, J. (2003). Historical and projected coastal Louisiana land changes: 1978-2050 (p. 39p). United States Geological Survey.

Barras, J. A. (2007). Satellite images and aerial photographs of the effects of Hurricanes Katrina and Rita on coastal Louisiana. US Department of the Interior, US Geological Survey.

Barras, J. A., Bernier, J. C., & Morton, R. A. (2008). Land Area Change in Coastal Louisiana, a Multidecadal Perspective (from 1956 to 2006) (p. 14). US Department of the Interior, US Geological Survey.

Barras, J. A., Brock, J. C., Morton, R. A., & Travers, L. J. (2010). Satellite images and aerial photographs of the effects of hurricanes Gustav and Ike on coastal Louisiana. US Geological Survey Data Series, 566.

Battjes, J. A. (1974). Surf similarity. Coastal Engineering Proceedings, 1(14).

Bradford, S. F. (2000). Numerical simulation of surf zone dynamics. Journal of waterway, port, coastal, and ocean engineering, 126(1), 1-13.

Boesch, D. F., Josselyn, M. N., Mehta, A. J., Morris, J. T., Nuttle, W. K., Simenstad, C. A., & Swift, D. J. (1994). Scientific assessment of coastal wetland loss, restoration and management in Louisiana. Journal of Coastal Research, i-103.

Bouma, T. J., Vries, M. D., Low, E., Kusters, L., Herman, P. M. J., Tanczos, I. C., & van Regenmortel, S. (2005). Flow hydrodynamics on a mudflat and in salt marsh vegetation: identifying general relationships for habitat characterisations. Hydrobiologia, 540(1-3), 259-274.

Baumann, R. H., Day, J. W., & Miller, C. A. (1984). Mississippi deltaic wetland survival: sedimentation versus coastal submergence. Science, 224(4653), 1093-1095.

Cahoon, D. R., & Reed, D. J. (1995). Relationships among marsh surface topography, hydroperiod, and soil accretion in a deteriorating Louisiana salt marsh. Journal of Coastal Research, 357-369.

Camfield, F. E. (1977). A method for estimating wind-wave growth and decay in shallow water with high values of bottom friction. (No. CERC-CETA-77-6). Coastal Engineering Research Center Fort Belvoir VA.

Chabreck, R. H., & Palmisano, A. W. (1973). The effects of Hurricane Camille on the marshes of the Mississippi River delta. Ecology, 1118-1123.

Chamberlain, J. L. (1959). Influence of Hurricane Audrey on the coastal marsh of southwestern Louisiana (No. TR-10-Pt-B). Louisiana State University Baton Rouge Coastal Studies Institute.

Chaney, P. L. (1998). Extratropical storms of the Gulf of Mexico and their effects along the northern shores of a barrier island: West Ship Island, Mississippi. Baton Rouge, Louisiana: Louisiana State University (Doctoral dissertation, Ph. D. dissertation, 159p).

Chopakatla, S. C., Lippmann, T. C., & Richardson, J. E. (2008). Field verification of a computational fluid dynamics model for wave transformation and breaking in the surf zone. Journal of waterway, port, coastal, and ocean engineering, 134(2), 71-80.

Church, J. A., & White, N. J. (2006). A 20th century acceleration in global sea-level rise. Geophysical research letters, 33(1), L01602.

Coleman, J. M., Roberts, H. H., & Stone, G. W. (1998). Mississippi River delta: an overview. Journal of Coastal Research, 699-716.

Cooper, N. J. (2005). Wave dissipation across intertidal surfaces in the Wash Tidal Inlet, Eastern England. Journal of Coastal Research, 28-40.

Couvillion, B. R., Barras, J. A., Steyer, G. D., Sleavin, W., Fischer, M., Beck, H., ... & Heckman, D. (2011). Land Area Change in Coastal Louisiana (1932 to 2010). US Department of the Interior, US Geological Survey.

Crowder, R.B. (1995). The Wonders of the Weather, Australian Government Publishing Service, Canberra,Chapter 3, 46-48.

D'Alpaos, A., Lanzoni, S., Marani, M., & Rinaldo, A. (2007). Landscape evolution in tidal embayments: Modeling the interplay of erosion, sedimentation, and vegetation dynamics. Journal of Geophysical Research, 112(F1), F01008.

Dahl, T. E. (2000). Status and trends of wetlands in the conterminous United States 1986 to 1997. US Fish and Wildlife Service.

Dalrymple, R. A., Kirby, J. T., & Hwang, P. A. (1984). Wave diffraction due to areas of energy dissipation. Journal of waterway, port, coastal, and ocean engineering, 110(1), 67-79.

Day Jr, J. W., Reed, D., Suhayda, J. N., Kemp, G. P., Cahoon, D., Boumans, R. M., & Latif, N. (1988). Physical processes of marsh deterioration. Final Report: Critical Physical Processes of Wetland Loss, 1994(1994), 5-1.

Day Jr, J. W., Martin, J. F., Cardoch, L., & Templet, P. H. (1997). System functioning as a basis for sustainable management of deltaic ecosystems. Coastal Management, 25(2), 115-153.

Day, J. W., Britsch, L. D., Hawes, S. R., Shaffer, G. P., Reed, D. J., & Cahoon, D. (2000). Pattern and process of land loss in the Mississippi Delta: a spatial and temporal analysis of wetland habitat change. Estuaries, 23(4), 425-438.

Day, J. W., Boesch, D. F., Clairain, E. J., Kemp, G. P., Laska, S. B., Mitsch, W. J., ... & Whigham, D. F. (2007). Restoration of the Mississippi Delta: lessons from hurricanes Katrina and Rita. Science, 315(5819), 1679-1684.

Day, J. W., Kemp, G. P., Reed, D. J., Cahoon, D. R., Boumans, R. M., Suhayda, J. M., & Gambrell, R. (2011). Vegetation death and rapid loss of surface elevation in two contrasting Mississippi delta salt marshes: The role of sedimentation, auto compaction and sea-level rise. Ecological Engineering, 37(2), 229-240.

Dean, R. G., & Bender, C. J. (2006). Static wave setup with emphasis on damping effects by vegetation and bottom friction. Coastal Engineering, 53(2), 149-156.

DeLaune, R. D., Baumann, R. H., & Gosselink, J. G. (1983). Relationships among vertical accretion, coastal submergence, and erosion in a Louisiana Gulf Coast marsh. Journal of Sedimentary Research, 53(1), 147-157.

DeLaune, R. D., Nyman, J. A., & Patrick Jr, W. H. (1994). Peat collapse, ponding and wetland loss in a rapidly submerging coastal marsh. Journal of Coastal Research, 1021-1030.

Ellison, M., (2011). Subsurface controls on mainland marsh shoreline response during barrier island transgressive submergence University of New Orleans Theses and Dissertations. Paper 458.

Fagherazzi, S., Palermo, C., Rulli, M. C., Carniello, L., & Defina, A. (2007). Wind waves in shallow microtidal basins and the dynamic equilibrium of tidal flats. Journal of Geophysical Research: Earth Surface (2003–2012), 112(F2).

Fagherazzi, S., & Wiberg, P. L. (2009). Importance of wind conditions, fetch, and water levels on wave-generated shear stresses in shallow intertidal basins. Journal of Geophysical Research: Earth Surface (2003–2012), 114(F3).

Fagherazzi, S., & Priestas, A. M. (2010). Sediments and water fluxes in a muddy coastline: interplay between waves and tidal channel hydrodynamics. Earth Surface Processes and Landforms, 35(3), 284-293.

Fagherazzi, S., Kirwan, M. L., Mudd, S. M., Guntenspergen, G. R., Temmerman, S., D'Alpaos, A., ... & Clough, J. (2012). Numerical models of salt marsh evolution: Ecological, geomorphic, and climatic factors. Reviews of Geophysics, 50(1).

Feagin, R. A., Lozada-Bernard, S. M., Ravens, T. M., Möller, I., Yeager, K. M., & Baird, A. H. (2009). Does vegetation prevent wave erosion of salt marsh edges?. Proceedings of the National Academy of Sciences, 106(25), 10109-10113.

Feagin, R. A., Irish, J. L., Möller, I., Williams, A. M., Mousavi, M. E, & Colón-Rivera, R. J. (2011). Engineering properties of wetland plants with application to wave attenuation. Coastal Engineering 58, 251-255.

Feng, Z., & Li, C. (2010). Cold-front-induced flushing of the Louisiana Bays. Journal of Marine Systems, 82(4), 252-264.

FitzGerald, D. M., & Knight, J. (Eds.). (2005). High resolution morphodynamics and sedimentary evolution of estuaries (Vol. 8). Springer.

Fonseca, M. S., & Cahalan, J. A. (1992). A preliminary evaluation of wave attenuation by four species of seagrass. Estuarine, Coastal and Shelf Science, 35(6), 565-576.

Francalanci, S., Bendoni, M., Rinaldi, M., & Solari, L. (2013). Ecomorphodynamic evolution of salt marshes: Experimental observations of bank retreat processes. Geomorphology, 195, 53-65.

Frazier, D. E. (1967). Recent deltaic deposits of the Mississippi River: their development and chronology. Transactions Gulf Coast Association of Geological Societies. 17:287–315

Fredsøe, J., & Deigaard, R. (1992). Mechanics of coastal sediment transport (Vol. 3). World Scientific.

Georgiou, I. Y., FitzGerald, D. M., & Stone, G. W. (2005). The impact of physical processes along the Louisiana coast. Journal of Coastal Research, 72-89.

Haigh M.J. 1977. The use of erosion pins in the study of slope evolution. In: Shorter Technical Methods (II), Technical Bulletin No 18, British Geomorphological Research Group, Geo Books, Norwich, UK.

Holthuijsen, L. H. (2007). Waves in oceanic and coastal waters. Cambridge University Press.

Howes, N. C., FitzGerald, D. M., Hughes, Z. J., Georgiou, I. Y., Kulp, M. A., Miner, M. D., & Barras, J. A. (2010). Hurricane-induced failure of low salinity wetlands. Proceedings of the National Academy of Sciences, 107(32), 14014-14019.

Hunt, J. N. (1979). Direct solution of wave dispersion equation. Journal of the Waterway Port Coastal and Ocean Division, 105(4), 457-459.

Jevrejeva, S., Moore, J. C., Grinsted, A., & Woodworth, P. L. (2008). Recent global sea level acceleration started over 200 years ago?. Geophysical Research Letters, 35(8), L08715.

Kamphuis, J. W. (1975). Friction factor under oscillatory waves. Journal of the Waterways Harbors and Coastal Engineering Division, 101(2), 135-144.

Keen, T. R. (2002). Waves and currents during a winter cold front in the Mississippi bight, Gulf of Mexico: Implications for barrier island erosion. Journal of coastal research, 622-636.

Kirwan, M. L., & Murray, A. B. (2007). A coupled geomorphic and ecological model of tidal marsh evolution. Proceedings of the National Academy of Sciences, 104(15), 6118-6122.

Knauss, J. A. (1996). Introduction to physical oceanography. 2nd edition, Prentice Hall, Upper Saddle River, New Jersey.

Knutson, P. L., Brochu, R. A., Seelig, W. N., & Inskeep, M. (1982). Wave damping in *Spartina alterniflora* marshes. Wetlands, 2(1), 87-104.

Kobayashi, N., Raichle, A. W., & Asano, T. (1993). Wave attenuation by vegetation. Journal of waterway, port, coastal, and ocean engineering, 119(1), 30-48.

Koch, E. W., Barbier, E. B., Silliman, B. R., Reed, D. J., Perillo, G. M., Hacker, S. D., ... & Wolanski, E. (2009). Non-linearity in ecosystem services: temporal and spatial variability in coastal protection. Frontiers in Ecology and the Environment, 7(1), 29-37.

Leonard, L. A., & Reed, D. J. (2002). Hydrodynamics and sediment transport through tidal marsh canopies. Journal of Coastal Research, 36(2), 459-469.

Li, C., Weeks, E., & Blanchard, B. W. (2010). Storm surge induced flux through multiple tidal passes of Lake Pontchartrain estuary during Hurricanes Gustav and Ike. Estuarine, Coastal and Shelf Science, 87(4), 517-525.

Lima, S. F., Neves, C. F., & Rosauro, N. M. L. (2005). Damping of gravity waves by fields of flexible vegetation. In COASTAL ENGINEERING CONFERENCE (Vol. 30, No. 1, p. 491). ASCE AMERICAN SOCIETY OF CIVIL ENGINEERS.

Lin, P., & Liu, P. L. F. (1998). A numerical study of breaking waves in the surf zone. Journal of fluid mechanics, 359(1), 239-264.

Longuet-Higgins, M. S., & Stewart, R. W. (1964, August). Radiation stresses in water waves; a physical discussion, with applications. In Deep Sea Research and Oceanographic Abstracts (Vol. 11, No. 4, pp. 529-562). Elsevier.

Louisiana Coastal Wetlands Conservation and Restoration Task Force, 2010, The 2009 Evaluation Report to the U.S. Congress on the Effectiveness of Coastal Wetlands Planning, Protection and Restoration Act Projects.

Løvås, S. M., & Tørum, A. (2000, July). Effect of Submerged Vegetation Upon Wave Damping and Run-Up on Beaches: A Case Study on Laminaria Hyperborea. ASCE.

Lowe, R. J., Falter, J. L., Koseff, J. R., Monismith, S. G., & Atkinson, M. J. (2007). Spectral wave flow attenuation within submerged canopies: Implications for wave energy dissipation. Journal of geophysical research, 112(C5), C05018.

Marani, M., D'Alpaos, A., Lanzoni, S., & Santalucia, M. (2011). Understanding and predicting wave erosion of marsh edges. Geophysical Research Letters, 38(21), L21401.

Mariotti, G., & Fagherazzi, S. (2010). A numerical model for the coupled long-term evolution of salt marshes and tidal flats. Journal of Geophysical Research: Earth Surface (2003–2012), 115(F1).

Mariotti, G., S. Fagherazzi, P. L. Wiberg, K. J. McGlathery, L. Carniello, & A. Defina (2010), Influence of storm surges and sea level on shallow tidal basin erosive processes, Journal of Geophysical Research., 115, C11012.

Martinez, L., O'Brien, S., Bethel, M., Penland, S., & Kulp, M. (2009). Louisiana Barrier Island Comprehensive Monitoring Program (BICM) Volume 2: Shoreline Changes and Barrier Island Land Loss 1800's-2005. Pontchartrain Institute for Environmental Sciences. New Orleans, Louisiana.

Massel, S. R., Furukawa, K., & Brinkman, R. M. (1999). Surface wave propagation in mangrove forests. Fluid Dynamics Research, 24(4), 219-249.

Mazda, Y., Magi, M., Ikeda, Y., Kurokawa, T., & Asano, T. (2006). Wave reduction in a mangrove forest dominated by Sonneratia sp. Wetlands Ecology and Management, 14(4), 365-378.

Mendez, F. J., & Losada, I. J. (2004). An empirical model to estimate the propagation of random breaking and nonbreaking waves over vegetation fields. Coastal Engineering, 51(2), 103-118.

Moeller, C. C., Huh, O. K., Roberts, H. H., Gumley, L. E., & Menzel, W. P. (1993). Response of Louisiana coastal environments to a cold front passage. Journal of Coastal Research, 434-447.

Moeller, I., Spencert, T., & French, J. R. (1996). Wind wave attenuation over saltmarsh surfaces: Preliminary results from Norfolk, England. Journal of Coastal Research, 1009-1016.

Möller, I., Spencer, T., French, J. R., Leggett, D. J., & Dixon, M. (1999). Wave transformation over salt marshes: a field and numerical modelling study from North Norfolk, England. Estuarine, coastal and shelf science, 49(3), 411-426.

Möller, I., & Spencer, T. (2002). Wave dissipation over macro-tidal saltmarshes: Effects of marsh edge typology and vegetation change. Journal of Coastal Research, 36, 506-521.

Möller, I. (2006). Quantifying saltmarsh vegetation and its effect on wave height dissipation: Results from a UK East coast saltmarsh. Estuarine, Coastal and Shelf Science, 69(3), 337-351.

Möller, I., Mantilla-Contreras, J., Spencer, T., & Hayes, A. (2011). Micro-tidal coastal reed beds: Hydro-morphological insights and observations on wave transformation from the southern Baltic Sea. Estuarine, Coastal and Shelf Science, 92(3), 424-436.

Morris, J. T., Sundareshwar, P. V., Nietch, C. T., Kjerfve, B., & Cahoon, D. R. (2002). Responses of coastal wetlands to rising sea level. Ecology, 83(10), 2869-2877.

Mossa, J., & Roberts, H. H. (1990). Synergism of riverine and winter storm-related sediment transport processes in Louisiana's coastal wetlands. AAPG Bulletin (American Association of Petroleum Geologists);(USA), 74(CONF-9010204).

Mudd, S. M. (2011). The life and death of salt marshes in response to anthropogenic disturbance of sediment supply. Geology, 39(5), 511-512.

Mullarney, J. C., & Henderson, S. M. (2010). Wave-forced motion of submerged single-stem vegetation. Journal of Geophysical Research: Oceans (1978–2012), 115(C12).

Muller, R. A., & Stone, G. W. (2001). A climatology of tropical storm and hurricane strikes to enhance vulnerability prediction for the southeast US coast. Journal of Coastal Research, 949-956.

Neumeier, U., & Ciavola, P. (2004). Flow resistance and associated sedimentary processes in a Spartina maritima salt-marsh. Journal of Coastal Research, 435-447.

Neumeier, U. (2007). Velocity and turbulence variations at the edge of saltmarshes. Continental Shelf Research, 27(8), 1046-1059.

Neumeier, U., Ferrarin, C., Amos, C. L., Umgiesser, G., & Li, M. Z. (2008). Sedtrans05: An improved sediment-transport model for continental shelves and coastal waters with a new algorithm for cohesive sediments. Computers & Geosciences, 34(10), 1223-1242

Nyman, J. A., DeLaune, R. D., & Patrick Jr, W. H. (1990). Wetland soil formation in the rapidly subsiding Mississippi River deltaic plain: Mineral and organic matter relationships. Estuarine, Coastal and Shelf Science, 31(1), 57-69

Penland, S.; Beall, A.; Britsch, L.D., III, & Williams, S.J., (2002). Geologic classification of coastal land loss between 1932 and 1990 in the Mississippi River Delta Plain, southeastern Louisiana. Gulf Coast Association of Geological Societies Transaction, 52, 799–807.

Penland, S., Wayne, L. D., Britsch, L. D., Williams, S. J., Beall, A. D., & Butterworth, V. C. (2000) The Processes of Coastal Land Loss in the Mississippi River Delta Plain. New Orleans, LA: USGS. USGS Open-File Report 00-0418.

Penland, S., Beale, A., & Kindinger, J. (2002). Environmental Atlas of Lake Pontchartrain Basin. USGS Open File Report 02-206.

Pant, H. R. (2013). Erosional resistance of cohesive sediments in coastal saltmarshes. MS Thesis, Louisiana State University 109 pp.

Pepper, D. A., & Stone, G. W. (2004). Hydrodynamic and sedimentary responses to two contrasting winter storms on the inner shelf of the northern Gulf of Mexico. Marine Geology, 210(1), 43-62.

Poore, R. Z., DeLong, K. L., Richey, J. N., & Quinn, T. M. (2009). Evidence of multidecadal climate variability and the Atlantic Multidecadal Oscillation from a Gulf of Mexico sea-surface temperature-proxy record. Geo-Marine Letters, 29(6), 477-484.

Priestas, A. M., and Fagherazzi, S., (2011). Morphology and hydrodynamics of wave-cut gullies, Geomorphology, 131(1–2), 1–13, doi:10.1016/j.geomorph.2011.04.004.

Reed, D. J. (1989). Patterns of sediment deposition in subsiding coastal salt marshes, Terrebonne Bay, Louisiana: the role of winter storms. Estuaries, 12(4), 222-227.

Reed, D. J. (1995). The response of coastal marshes to sea-level rise: Survival or submergence? Earth Surface Processes and Landforms, 20, 39–48.

Reed, D. J., Davidson-Arnott, R., & Perillo, G. M. (2009). Estuaries, coastal marshes, tidal flats and coastal dunes. Geomorphology and Global Environmental Change, Slaymaker O, Spencer T, Embleton-Hamann C (eds). Cambridge University Press: Cambridge, 130-157.

Roberts H. H., Huh, O. K., Hsu, S. A., Rouse, L .J. Jr. & Rickmand, D. (1987). Impact of cold-front passageson geomorphic evolution and sediment dynamics of the complex Louisiana coast. Coastal Sediments '87, Proceedings of a Specialty Conference (May 12-14, 1987, New Orleans, Louisiana). American Society of Civil Engineers, New York, pp. 1950-1963.

Roberts, H. H. (1997). Dynamic changes of the Holocene Mississippi River delta plain: the delta cycle. Journal of Coastal Research, 605-627.

Quartel, S., Kroon, A., Augustinus, P. G. E. F., Van Santen, P., & Tri, N. H. (2007). Wave attenuation in coastal mangroves in the Red River Delta, Vietnam. Journal of Asian Earth Sciences, 29(4), 576-584.

Schindler, J. (2010). Estuarine Dynamics as a Function of Barrier Island Transgression and Wetland Loss: Understanding the Transport and Exchange Processes. University of New Orleans Theses and Dissertations. Paper 1260. http://scholarworks.uno.edu/td/1260

Schwimmer, R. A. (2001). Rates and processes of marsh shoreline erosion in Rehoboth Bay, Delaware, USA. Journal of Coastal Research, 672-683.

Schwimmer, R. A., & Pizzuto, J. E. (2000). A model for the evolution of marsh shorelines. Journal of Sedimentary Research, 70(5), 1026-1035.

Singh, A., & Aung, T. (2005). Effect of barometric pressure on sea level variations in the Pacific region. The South Pacific Journal of Natural and Applied Sciences, 23(1), 9-15.

Smith, J. M., Jensen, R. E., Kennedy, A. B., Dietrich, J. C. & Westerink, J. J. (2011). Waves in wetlands: Hurricane Gustav. Proceedings of the 32nd International Conference on Coastal Engineering (ICCE 2011).

Steyer, G. D., Cretini, K. F., Piazza, S., Sharp, L. A., Snedden, G. A., & Sapkota, S. (2010). Hurricane influences on vegetation community change in coastal Louisiana. U. S. Geological Survey.

Stone, G. W., Liu, B., Pepper, D. A., & Wang, P. (2004). The importance of extratropical and tropical cyclones on the short-term evolution of barrier islands along the northern Gulf of Mexico, USA. Marine Geology, 210(1), 63-78.

Tambroni, N., & Seminara, G. (2012). A one-dimensional eco-geomorphic model of marsh response to sea level rise: Wind effects, dynamics of the marsh border and equilibrium. Journal of Geophysical Research: Earth Surface (2003–2012), 117(F3).

Tonelli, M., Fagherazzi, S., & Petti, M. (2010). Modeling wave impact on salt marsh boundaries. Journal of Geophysical Research: Oceans (1978–2012), 115(C9).

Törnqvist, T. E., Kidder, T. R., Autin, W. J., van der Borg, K., de Jong, A. F., Klerks, C. J., & Wiemann, M. C. (1996). A revised chronology for Mississippi River subdeltas. Science, 273(5282), 1693-1696.

Trenhaile, A. S. (2009). Modeling the erosion of cohesive clay coasts. Coastal Engineering, 56(1), 59-72.

Tschirky, P., Hall, K., & Turcke, D. (2001). Wave attenuation by emergent wetland vegetation. In COASTAL ENGINEERING CONFERENCE (Vol. 1, pp. 865-877). ASCE AMERICAN SOCIETY OF CIVIL ENGINEERS.

Tucker, M. J., & Pitt, E. G. (2001). Waves in ocean engineering. Elsevier Ocean Engineering Book Series, 5, Elsevier: Amsterdam.

U.S. Army Corps of Engineers, (1984). Shore Protection Manual, Volume 2, Coastal Engineering Research Center (U.S.).

USEPA. 1999. Ecological condition of estuaries in the Gulf of Mexico. EPA 620-R-98-004. U.S. Environmental Protection Agency, Office of Research and Development, National Health and Environmental Effects Research Laboratory, Gulf Ecology Division, Gulf Breeze, Florida. 80 pp.

van Eerdt, M.M. (1985). The influence of vegetation on erosion and accretion in salt marshes of the Oosterschelde, The Netherlands. Vegetatio, 62, 362-373.

van de Koppel, J., van der Wal, D., Bakker, J. P., & Herman, P. M. (2005). Self-organization and vegetation collapse in salt marsh ecosystems. The American Naturalist, 165(1), E1-E12.

Watzke, D. A. (2004). Short-term Evolution of a Marsh Island System and the Importance of Cold Front Forcing, Terrebonne Bay, Louisiana. MS Thesis, Louisiana State University 42 pp.

Wayne, C. J. (1976). The effects of sea and marsh grass on wave energy. Coastal Research Notes, 4(7), 6-8.

Williams, S.J., 1995, Louisiana coastal wetlands: A resource at risk: U.S, Geological Survey, Marine and Coastal Geology Program, Reston, VA.

Willmott, C. J. (1981). On the validation of models. Physical geography, 2(2), 184-194.

Wilson, C. A., & Allison, M. A. (2008). An equilibrium profile model for retreating marsh shorelines in southeast Louisiana. Estuarine, Coastal and Shelf Science, 80(4), 483-494.

Wu, W., Y. Ozeren, D. Wren, Q. Chen, G. Zhang, M. Holland, Y. Ding, S.N. Kuiry, M. Zhang, R. Jadhav, J. Chatagnier, Y. Chen, & L. Gordji. (2011). Investigation of surge and wave reduction by vegetation. Phase I Report for SERRI Project No. 80037, The University of Mississippi, MS, p. 315.

Wu, W., Ozeren, Y., Wren, D., Chen, Q., Zhang, G., Holland, M., & Chen, Y. (2012). Investigation of surge and wave reduction by vegetation: Phase I Report for SERRI Project No. 80037, The University of Mississippi, MS, p. 397.

Wunsch, C., & Stammer, D. (1997). Atmospheric loading and the oceanic "inverted barometer" effect. Reviews of Geophysics, 35(1), 79-107.

Yang, S. L., Shi, B. W., Bouma, T. J., Ysebaert, T., & Luo, X. X. (2012). Wave attenuation at a salt marsh margin: A case study of an exposed coast on the Yangtze Estuary. Estuaries and coasts, 35(1), 169-182.

Young, I. R., & Verhagen, L. A. (1996). The growth of fetch limited waves in water of finite depth. Part 1. Total energy and peak frequency. Coastal Engineering, 29(1), 47-78.

Yuill, B., Lavoie, D., & Reed, D. J. (2009). Understanding subsidence processes in coastal Louisiana. Journal of Coastal Research, 23-36.

Vita

Kevin Trosclair is a native of South Louisiana and was raised in lower Plaquemines Parish. He earned a Bachelor's Degree in Nursing from Louisiana State University and enjoyed several years traveling and working throughout the western U.S. He returned to Louisiana to pursue a Master's Degree in Earth and Environmental Sciences under Dr. Ioannis Georgiou. He will begin employment in the petroleum industry in 2013.